Microcavity Development for the Control of Erbium-Doped Silicon Luminescence

James S. Foresi and Lionel C. Kimerling

Department of Materials Science and Engineering
Massachusetts Institute of Technology
Cambridge, MA 02139

Contractor: **Massachusetts Institute of Technology**
Contract Number: **F49620-93-1-0481**
Effective Date of Contract: **15 August 1993**
Contract Expiration Date: **14 December 1996**

REPORT DOCUMENTATION PAGE

AFOSR-TR-97

0140

1. AGENCY USE ONLY (Leave blank)	2. REPORT DATE	3. REPORT TYPE AND DATES COVERED
		FINAL REPORT 15 Aug 93 - 14 Dec 96

4. TITLE AND SUBTITLE
(AASERT-93) Silicon Germanium Alloy Heterostructures for Optoelectronics

5. FUNDING NUMBERS
61103D
3484/TS

6. AUTHOR(S)
Professor Kimerling

7. PERFORMING ORGANIZATION NAME(S) AND ADDRESS(ES)
Massachusetts Institute of Technology
Materials Science and Engineering
Cambridge, MA 02139

8. PERFORMING ORGANIZATION REPORT NUMBER

9. SPONSORING/MONITORING AGENCY NAME(S) AND ADDRESS(ES)
AFOSR/NE
110 Duncan Avenue Suite B115
Bolling AFB DC 20332-8050

10. SPONSORING/MONITORING AGENCY REPORT NUMBER
F49620-93-1-0481

11. SUPPLEMENTARY NOTES

12a. DISTRIBUTION/AVAILABILITY STATEMENT
APPROVED FOR PUBLIC RELEASE: DISTRIBUTION UNLIMITED

12b. DISTRIBUTION CODE

13. ABSTRACT *(Maximum 200 words)*

This program, Microcavity Development for the Control of Erbium-Doped Silicon Luminescence, has discovered that the Si/SiO_2 materialas system has outstanding promise as a medium for the generation and confinement of light. Materials and processing methods for the fabrication of microcavity devices compatible with erbium-doped silicon (Si:Er) were developed. We have demonstrated two types of silicon based microcavities for the control of spontaneous emission from Si:Er which involves: Light guiding in highly confining, submicron dimensioned wilicon waveguides. the microdisk and PBG cavities, when coupled to waveguides, can act as filters, signal routers, and compact gain sections for integrated laser devices. The use of a high index difference system such as $SiSiO_2$ allows the reduction of the dimensions of waveguides and associated optical components to the submicron range. This reduction in size provides for integration of higher densities and greater functionality on a single die. This program has provided the foundation for a complete, submicron scaled silicon integrated optics technology.

14. SUBJECT TERMS			15. NUMBER OF PAGES
			16. PRICE CODE
17. SECURITY CLASSIFICATION OF REPORT	18. SECURITY CLASSIFICATION OF THIS PAGE	19. SECURITY CLASSIFICATION OF ABSTRACT	20. LIMITATION OF ABSTRACT
UNCLASSIFIED	UNCLASSIFIED	UNCLASSIFIED	

Contents

List of Figures

List of Tables

1 Executive Summary

This program, Microcavity Development for the Control of Erbium-Doped Silicon Luminescence, has discovered that the Si/SiO_2 materials system has outstanding promise as a medium for the generation and confinement of light. Materials and processing methods for the fabrication of microcavity devices compatible with erbium-doped silicon (Si:Er) were developed. Light guiding in highly confining, submicron dimensioned silicon waveguides was demonstrated for the first time. This program has provided the foundation for a complete, submicron scaled silicon integrated optics technology.

The objective of the program was the development of optical devices that are compatible with the well-established processing capability of Si electronics. This compatibility offers a pathway for integration of fast optical interconnects with silicon electronics and provides a basis for horizontally integrated resonant structures such as microcavities. The large index difference of the Si/SiO_2 materials system ($\Delta n \approx 2.0$) provides for high confinement of light for microphotonic integration at submicron length scales.

During the course of this program we developed submicron cross-section optical waveguides in silicon, as well as microdisk and photonic band gap (PBG) microcavities. The waveguides, with cross-sections of $0.2 \times 0.5 \mu m$, are the smallest ever measured. We have coupled light into these small structures and measured both the materials and processing related dependences of loss. The critical parameter for controlling losses in these submicron guides is sidewall roughness. Light emission at $\lambda = 1.54 \mu m$ from Si:Er microdisks was measured by cathodoluminesence at 4K. PBG microcavities were fabricated with band gaps centered at $\lambda = 5.0 \mu m$ and $\lambda = 1.54 \mu m$. The $\lambda = 5.0 \mu m$ devices were employed as input and output waveg-

uide couplers for light of λ=1.54μm. This property of the PBG devices provides grating-like couplers that are an order of magnitude smaller in size than typical grating coupler devices. PBG microcavities at λ=1.54μm with minimum feature sizes of 0.10μm were fabricated using e-beam and x-ray lithography. An evaluation system for testing the throughput of the PBG devices as a function of wavelength was developed.

Dimensional control is critical to the operation of both the microdisk and PBG microcavities. In order to enhance the spontaneous emission rate of Si:Er it is necessary to overlap the resonant mode of the microcavity with the Si:Er luminesence peak. Analysis of the microdisk mode position as a function of disk radius and thickness showed that the overlap requires exacting tolerances. We developed a unique test structure for evaluating the mode position that does not rely on luminescence. The structure, a microdisk coupled to waveguides, can also be used as a channel dropping filter for wavelength division multiplexing applications.

Silicon-on-insulator (SOI) technology is critical to the development of planar Si/SiO_2 optical components. The design of planar microcavities places constraints on the buried oxide and top silicon layer thickness that few SOI technologies can achieve. We developed polycrystalline Si as an alternative light confining medium that is free of the process constraints of SOI technology. By investigating the loss mechanisms in polySi we reduced the optical losses at λ=1.54μm from 75dB/cm to 15dB/cm. Critical to the reduction of the losses are control of the surface roughness of the polySi (which was found to contribute 40dB/cm of loss) and passivation of the dangling bonds in the material (which were found to contribute 20dB/cm of loss). For this deposition-based technology, the layer thicknesses of both the guiding layer and the buried SiO_2 can be varied appreciably, and multilayer, vertically in-

tegrated structures are possible. PolySi is ubiquitous on Si fablines and has the additional advantage that it removes the need for exotic substrates.

The research performed in this program has pioneered new areas of research that allow the miniaturization of optical components in a materials system compatible with standard silicon IC processing. The microdisk and PBG cavities, when coupled to waveguides, can act as filters, signal routers, and compact gain sections for integrated laser devices. The use of a high index difference system such as Si/SiO_2 allows the reduction of the dimensions of waveguides and associated optical components to the submicron range. This reduction in size provides for integration of higher densities and greater functionality on a single die. These optical device dimensions, on the scale of electronic devices of Si integrated circuits, stand at the gateway of an integrated optics technology that is not limited by yield or the reduced functionality of large devices.

2 Introduction

Erbium-doped silicon is a promising light emitting materials system that can lead to the development of an optoelectronics technology compatible with integrated circuit processing. The emission from erbium has a number of advantages: emission at λ=1.54μm, which is compatible with optical fiber, a narrow spectrum (100$\AA$ at 300K), and no dependence of wavelength on temperature. Light emitting diodes have been fabricated in Er-doped Si and these devices have been operated up to 300K with measurable optical output. However, the emission at room temperature is greatly reduced from the emission at cryogenic temperatures. The temperature quenching that occurs is linked to the existence of fast competitive non-radiative recombination processes. Microcavity devices have been shown to allow control of radiative emission rates and the focus of the research presented here is to develop microcavity devices in silicon. Two microcavity devices were developed: microdisk and photonic band gap microcavities. The remainder of this report presents the physics of light emission from Er-doped silicon, the operation of microcavity devices, the development of silicon microcavities and the control of erbium emission using the devices.

2.1 Light emission from erbium-doped silicon

Silicon is an indirect band gap semiconductor. Optical emission from an indirect band gap material requires that a phonon with the proper momentum be available when an electron moves from the conduction to the valence band. The phonon requirement makes light emission in silicon a low probability, three particle process. Direct band gap materials, such as GaAs and GaN, require no phonon for the transition from conduction band to valence band

making light emission much more efficient. Despite the indirect band gap, several successful methods of achieving silicon light emission have been devised. These include doping silicon with isoelectronic centers [1], making porous [2] or nanocrystalline [3] silicon to localize the electrons and make the optical transitions behave as they would in a direct band gap material, and doping silicon with erbium [4]. Erbium doping provides the most robust and most integrated circuit process compatible method for producing efficient luminescence from silicon. Erbium-doped silicon has been demonstrated, by our group [5] and independently [6], to produce luminescence at room temperature. It is also fully compatible with existing silicon integrated circuit fabrication [5] and has the added advantage of emitting at a wavelength of 1.54μm. This wavelength matches well the low loss fiber optic window at 1.55μm and makes erbium doped silicon compatible with existing fiber optic communication systems. This luminescence occurs between core levels of the f-shell and is therefore largely independent of the erbium host material and the temperature.

Erbium can be incorporated into silicon either by ion implantation or by doping during growth. In either case, the luminescence is greatly enhanced if a ligand, such as oxygen, is used to codope the silicon. A typical spectrum of erbium-doped silicon is shown in Figure 1. This sample was coimplanted with erbium and oxygen and the spectrum is taken at 4K. The spectrum shows a sharp peak at λ=1.54μm with several peaks at longer wavelengths. These longer wavelength peaks are suspected to be associated with the ligand field splitting of the core levels that results from the formation of specific erbium-oxygen complexes in the silicon. When the erbium is incorporated using ion implantation, an anneal step is necessary to remove implant damage and to allow the erbium and oxygen to form optically

active complexes. Anneal schedules depend on implant energies and doses, but are typically 800C for 30minutes. Ion implantation limits the peak concentration to the solubility limit of erbium in silicon (typically $10^{16}cm^{-3}$). When erbium is incorporated during growth, metastable concentrations of erbium greater than $10^{20}cm^{-3}$ can be achieved and no anneal step is required.

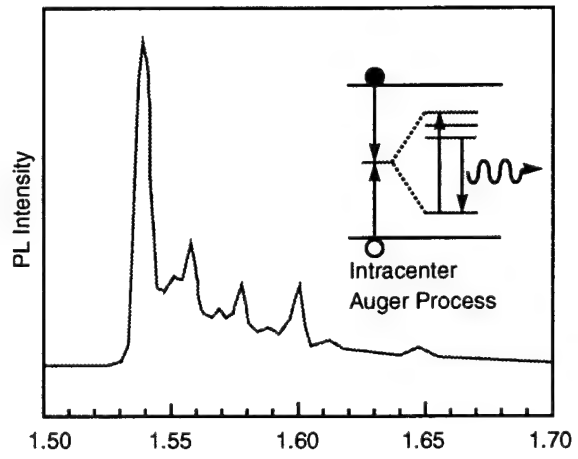

Figure 1: Low temperature (4K) Si:Er photoluminescence. Samples are doped with $5x10^{17}cm^{-3}$ Er and $1x10^{18}cm^{-3}$ O and annealed for 30min at 800°C. The excitation source is a 488nm Ar ion laser.

Regardless of the method of incorporation, the intensity of the erbium luminescence falls off rapidly at temperatures over 100K. This quenching limits the usefulness of erbium-doped silicon for practical devices. Competitive, non-radiative mechanisms involving energy back-transfer from the excited core levels are responsible for the intensity reduction at higher temperatures. The nature of these non-radiative mechanisms varies as the temperature increases. In the range from 70K to 150K, free carriers not taking part in luminescence receive the energy from the excited erbium prior to luminescence. At temperatures above 150K, it is expected that multi-phonon processes can deexcite the erbium.

To limit the core level effects of the free-carrier or phonon processes, it is necessary to

increase the spontaneous emission rate of the erbium (decrease the excited state lifetime). Increasing the spontaneous emission rate can be accomplished either by engineering the local environment around the erbium (e.g., through optimizing the ligand field), or by incorporating the erbium in a resonant cavity tuned to the emission frequency. The physics of resonant cavities, and their effect on spontaneous emission rates is covered in the next section.

2.2 Control of spontaneous emission

The fall-off of erbium luminescence at ambient temperatures is a result of competing recombination processes which have lifetimes shorter than that of the erbium excited state [6, 7, 8]. One method of probing the effect of lifetime is to incorporate the Si:Er into a microcavity. A microcavity consists of highly reflective walls which confine emission within a small volume (on the order of λ^3 where λ is the emission wavelength). Microcavities have been shown, theoretically and experimentally [9, 10], to allow control of the spontaneous emission rate. The most relevant of this work was performed in microcavities containing erbium-doped SiO_2 where 'giant' enhancements of the erbium luminescence were seen [11, 12].

Microcavities in other semiconducting systems, most notably the GaAs/AlGaAs system, are primarily made by creating dielectric stacks which act as mirrors [10, 13, 14]. These structures can be made by MOCVD or MBE techniques. The thicknesses of the layers in the stacks must be $\lambda/4n$ where n is the refractive index of the material. The number of layers required to make a highly reflective stack depends on the refractive index difference between the layers of the stack. Layers with large Δn require only a few layer pairs. Making such structures with crystalline materials requires a well lattice-matched material system

to achieve $\lambda/4n$ layer thicknesses with a large enough Δn to keep the number of layers reasonable. If crystallinity is not a requirement for good light emission (as in the Er doped SiO_2 microcavities which are amorphous [11]), then lattice matching is not required and the Δn's can be high with no concern for epitaxy. Dielectric stacks could be considered in the Si/SiGe system, but this system is not lattice-matched. A large number of small Δn layers would have to be used and using multilayers detracts from the compatibility with standard IC processing. Data concerning light emission from polycrystalline and amorphous Si:Er is presented later in this report and these materials could be used for vertical microcavities.

Multilayer microcavities result in vertically integrated light emitters. To be of use the light from these microcavities must be coupled into a waveguide either by fiber optic or by a free space coupling scheme. Coupling a light emitting source to a waveguide always results in added complexity and optical loss. If possible, it would be better to integrate the microcavity directly into a waveguide device.

In this study two waveguide-integrable structures for Si:Er microcavities are investigated. Both of these structures rely on silicon-on-insulator (SOI) technology, but they use only standard silicon processing technologies with no multilayer epitaxy. The first structure, a microdisk microcavity, consists of a silicon disk with a radius of approximately 1.0μm and thickness of 0.2μm [15]. The edge of the disk serves as the mirror in this structure and light traveling around the disk is confined by total internal reflection. This microcavity requires minimal processing. The second microcavity makes use of photonic band gap (PBG) technology. PBG technology uses periodic variations in dielectric constant to create reflective structures [16, 17]. PBG microcavities can be integrated directly into a waveguide which

eliminates the need for any additional coupling schemes.

2.3 Report organization

The remainder of this report includes background on the temperature dependence of Si:Er luminescence, information concerning the fabrication of microdisk microcavities and a discussion of the issues involved in the fabrication and testing of PBG structures. These are followed by a description of the completed work. A conclusion describing how this research will contribute to the future of light emitting is presented.

3 Background

This section includes discussions concerning the temperature dependence of Si:Er luminescence. The role of spontaneous emission rate is included in the discussion and the use of microcavities to enhance the spontaneous emission rate is detailed. The microdisk microcavity design is presented and a primer on the theory and fabrication of photonic band gap (PBG) structures concludes the background section.

3.1 Si:Er luminescence temperature dependence

Erbium luminescence in silicon is quenched as temperatures are increased from 77K to 300K. This quenching has been reported by three independent laboratories [7, 18, 19] and is found to have an activation energy from 0.13 to 0.16eV. The activation energy is not dependent on codopant, processing conditions or Er concentration. however a dependence on annealing temperatures was found [7]. Higher annealing temperatures shift the onset of quenching

to higher temperatures. Coffa, et al [18] found a direct correlation between the photoluminescence intensity and the lifetime (Figure 2). These data indicate that competitive, non-radiative processes occur at high temperatures. Non-radiative paths are reduced by annealing, explaining the shift to higher onset temperatures with annealing temperature. Additionally, long lifetime processes will not be evident if faster processes are available for recombination; this would account for the reduction in light output with a decrease in the photoluminescence lifetime.

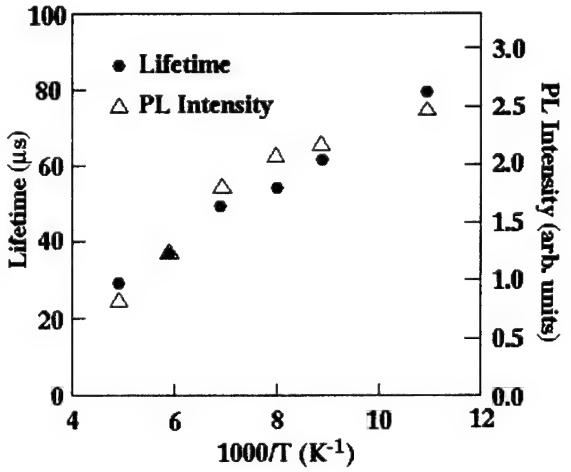

Figure 2: Temperature dependence of photoluminescence peak intensity and photoluminescence lifetime of Si:Er. From reference [7].

As the temperature is increased, the photoluminescence spectrum of Si:Er changes. The main peak at 1.54μm broadens and satellite peaks appear (Figure 3). The broadening of the main peak is attributed to homogenous broadening due to thermal vibration. The satellite peaks are attributed to thermal population of high stark levels of $I_{13/2}$ [7]. The broadening of the peak and the evolution of satellite peaks are undesirable for optical communication as it is possible for the effective index of the waveguide to vary as a function of wavelength. This waveguide dispersion can broaden pulses and limit data rates. The thermal quenching and

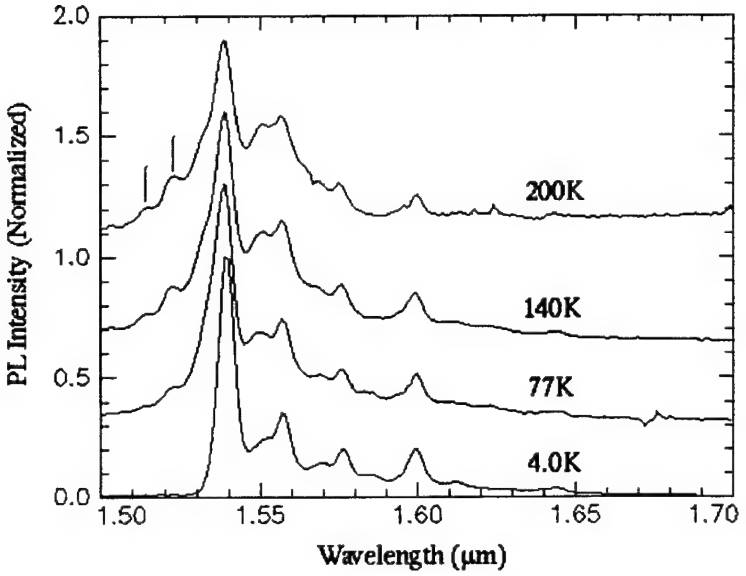

Figure 3: Photoluminescence spectrum evolution of Si:Er with increasing temperature. Short wavelength peaks attributed to thermally populated upper manifold states of the Er.

spectrum broadening effects are evident in Si:Er made by both MBE and ion implantation, as well they are evident in other Er doped systems such as $In_{1-x}Ga_xP$ [20].

Microcavities can alleviate the effects of high temperature on the emission characteristics of Si:Er. By confining the emission of the erbium to a small volume with a well defined resonance, the excited state lifetime can be reduced and the spectrum can be narrowed. As well, confinement in a microcavity will alter the spatial radiation pattern of the Si:Er. While typical spontaneous emission is isotropic, emission in a microcavity is enhanced along the direction of the reflecting walls that form the microcavity. The effects of microcavities are discussed in the next section.

3.2 Controlling luminescence with microcavities

The spontaneous emission rate, spatial radiation pattern and spectrum of a light emitting medium can be controlled using a microcavity. Microcavities control these properties by modifying the coupling of the light emitting medium with the vacuum field. The ability to alter this coupling has far reaching implications which are beyond the scope of this work, but are covered quite well elsewhere [21, 22, 23, 24, 25]. The details of the physics underlying spontaneous emission rate enhancement are also thoroughly explained in the available literature [9, 26, 27]. The results of the theoretical analysis (as presented by Yokoyama and Brorson [27]) are given here. If only one resonant cavity mode overlaps the spectrum of the light emitting medium the spontaneous emission rate, A_c, in a cavity is represented by:

$$A_c = \eta A \tag{1}$$

with

$$\eta = \frac{Qc^3}{4\pi\nu_0^3 V} \tag{2}$$

where A is the spontaneous emission rate with no cavity, ν_o is the transition frequency, Q is the cavity quality factor, c is the velocity of light, and V is the cavity mode volume.

The quality factor can be defined a number of equivalent ways. In the most general sense it is defined as the power stored in a microcavity divided by the power dissipated from the microcavity. For a Fabry-Perot microcavity which consists of identical parallel reflectors, the Q can be calculated from a knowledge of the wall reflectivities:

$$Q = \frac{\pi\sqrt{R}}{1-R}\frac{2l}{\lambda} \tag{3}$$

where R is the wall reflectivity and l is the wall separation. This definition of Q is only accurate for light normally incident on the walls. An additional, useful definition of Q is in terms of the resonance width of the cavity:

$$Q = \frac{f}{\Delta f} \tag{4}$$

where f is the center frequency of the resonance and Δf is the full width at half maximum (FWHM) of the resonance peak.

From equation (2) the requirements for spontaneous emission enhancement are seen to be a small cavity volume and a large quality factor. If the ratio of the Q of the cavity to the volume of the cavity is larger than approximately λ^3 then an enhancement of the spontaneous emission should occur. Microcavities have been fabricated in semiconductor materials due to the availability of fabrication techniques enabling the dimensional control of the submicron structures required to minimize V. Additionally, highly reflective structures can be made resulting in large Q's. Spontaneous emission enhancement has been reported in GaAs [10], dye-containing Langmuir-Blodgett films [28] and Er doped SiO_2 [12]. All of these applications used multi-layer dielectric stacks. Spontaneous emission rates were increased by about a factor of 2 in the GaAs and dye-containing structures and by a factor of 1.5 in the Er structures. Figure 2 shows that the spontaneous emission lifetime is reduced by a factor of 4 from 90K to 200K. If the spontaneous emission rate can be increased by a factor of 4,

the luminensence quenching should be effectively reduced.

Erbium luminescence in silicon is isotropic. There is no preferred direction for emission. In order to capture the majority of the emitted light a lensing arrangement must be used. While lensing will make the light output more directional, it will never successfully capture all of the light emission and what is not captured is essentially lost. Microcavities can be used to limit light emission to a narrow range of angles and facilitate capture of the majority of produced luminescence. The spatial radiation patterns from microcavities have been determined theoretically and experimentally. For planar microcavities, the theoretical calculations show that the directionality depends critically on the spacing of the walls [22] with more closely spaced walls (on the order of the radiation wavelength) resulting in more highly directional output. The directionality improvements have been experimentally verified in GaAs structures [13, 14] and Er:SiO_2 structures [12]. Yamamoto, et al, reported an enhancement of the spatial radiation pattern of 130 compared to that of an isotropic radiator.

Finally, spectral enhancements are expected from microcavities, even if lasing is not achieved. The cavity resonance channels all of the spontaneous emission into the cavity mode and this controls the output emission spectral width. The width of the cavity mode, and therefore the width of the output emission, is determined by the reflectivity of the cavity walls (see equations (3) and (4)). Reductions in linewidth by a factor of four have been reported in GaAs resonant cavity devices [14, 29]. Schubert reported data for a resonant cavity light emitting diode (LED) showing that, even without lasing, the linewidth was controlled by the cavity Q.

The most relevant of the microcavity work was presented by Vredenberg, et al [12]. They

constructed a Si/SiO_2 distributed Bragg structure with an Er implanted SiO_2 active cavity layer. Figure 4 shows the results of the photoluminescence tests. The erbium signal, which was broad and double peaked without a cavity, is only 10nm FWHM when in the cavity. Additionally, the strong angular dependence of the output intensity is obvious. Spontaneous emission rate enhancement was measured to be approximately 1.5.

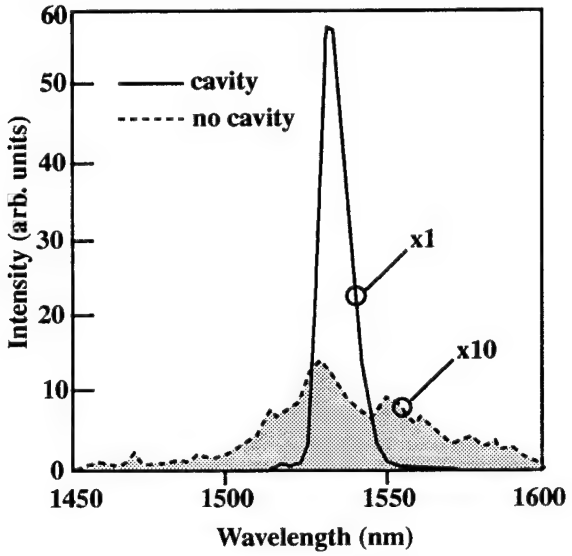

Figure 4: Effects of a microcavity structure on the spontaneous emission from Er doped SiO_2. From reference [12].

Microcavities offer improvements in three areas critical to Si:Er technology: spontaneous emission rate, directionality and spectral width. While these reasons alone are sufficient to warrant research in Si:Er microcavities there is added incentive in that increasing the spontaneous emission rate may lead to higher temperature operation. The next two sections describe the microcavities developed to modify the spontaneous emission from Si:Er.

3.3 Microdisk microcavities

The first microcavity design considered is the microdisk. This microcavity consists simply of a thin disk of a high refractive index material surrounded and supported by a low refractive index material. Light is confined in this structure by total internal reflection at the edge of the disk. The reason for considering this structure is that it represents perhaps the simplest possible microcavity design in silicon. The fabrication of such a structure requires only that SOI substrates be used. These substrates must consist of thin (2000$\AA$) layers of crystalline silicon separated from a silicon wafer by a layer of oxide. The top silicon is simply patterned and etched into microdisks. The SiO_2 limits the radiation of the disk mode into the underlying Si wafer.

Theoretical analysis of the propagation modes in microdisk structures have been published [15]. From this analysis it was found that the light propagating around the microdisk is confined near the edge of the disk and light is emitted from a narrow range of angles emanating from the disk edge. An additional feature is that the intensity decays exponentially out to a distance proportional to the radius and refractive index of the disk before propagating freely.

Microdisks have been fabricated in the InP/InGaAsP system [15, 30, 31]. These structures consisted of a series of InGaAs quantum wells separated by InGaAsP. The quantum wells were grown on an InP substrate which was then selectively etched with HCl. The HCl etched away the InP from underneath the microdisk leaving an InP post which supported the microdisk and kept it far enough from the substrate to eliminate losses to the substrate. Cavity Q's for these structures were measured and ranged from 100 to 750 [30]. Spectral

narrowing was measured even below the laser threshold.

The results for the InP/InGaAsP disks are impressive, but the Si/SiO_2 system should prove even better. The high index InP post which supports the InGaAsP quantum wells can actually couple light from the microdisk to the substrate. For silicon microdisks the structure is everywhere supported by relatively low index SiO_2. The leakage loss to the substrate can be reduced by increasing the SiO_2 thickness. We can expect that the largest source of loss from Si/SiO_2 microdisk microcavities will be due to roughness of the disk edge and surface. The surface roughness will depend on the starting SOI materials and the edge roughness depends on the masks, photolithography and etch processes used to create the disks.

Microdisk microcavities provide an excellent, easily fabricated tool for investigating the spectral and lifetime changes we can expect for Si:Er. To make the structures technologically useful requires a novel method of coupling the light out. Most of the published experimental results come from measuring the spectrum of the light scattered from the surface of the structure. Small gratings have been formed on the edge of the disk to enhance output coupling [30], but this still does not make use of the directionality enhancements available from more standard microcavity designs. In the results section of this report, designs for coupling light from a microdisk into a waveguide are presented. In the next section we will discuss another microcavity design which has excellent directionality and coupling characteristics.

3.4 Photonic band gap structures

One method of making highly reflective structures in dielectrics is to employ Photonic Band Gap (PBG) technology [32]. PBG materials consist of periodic dielectric lattices. A photon

traveling through such a lattice encounters a periodic variation in dielectric constant analogous to the periodic potential encountered by an electron traveling through a semiconductor lattice. As in the case of semiconductors, there arises a band of frequencies which are not allowed to propagate and are completely reflected by the material. Photonic band gaps have been investigated theoretically in three dimensional structures [33, 34, 35, 36, 37], two dimensional structures [38, 39] and one dimensional structures (an analogy to the Kronig-Penney model of periodic potentials in one dimension) [39]. While a large number of theoretical investigations have been published, the experimental work has lagged. This is primarily due to the small device structures and difficult geometries required for PBG materials working at optical frequencies [40]. Some experimental work has been performed at microwave frequencies and the agreement with theoretical calculations is found to be quite good [32, 39, 41]. Figure 5 shows experimental results for 3-D PBG material fabricated for use at microwave frequencies. The first plot shows the existence of a 'forbidden gap' or range of frequencies which was not allowed to propagate through the structure. The second plot shows the existence of a gap state. This state was created by including a 'defect' in the PBG structure. The defects in these structures are introduced by either including additional dielectric material or by removing dielectric material. These defect states are actually resonant cavity modes. The Q of the defect mode shown in Figure 5 was estimated to be 1000 [32]. These high Q modes can be used to create PBG microcavities for Si:Er.

A requirement for the existence of a photonic band gap is a large dielectric contrast for the materials which are used. The dielectric contrast is defined as ϵ_1/ϵ_2 where ϵ_1 is the larger dielectric constant. This is again analagous with semiconductor systems where large

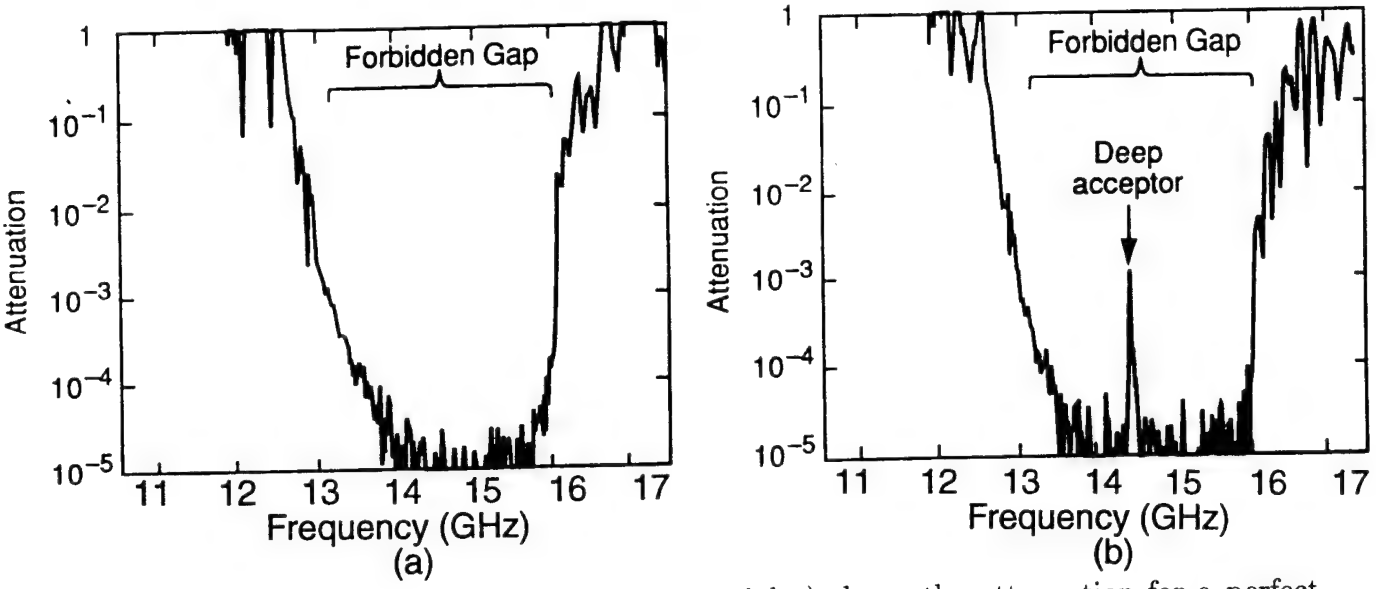

Figure 5: Attenuation data for 3-D PBG material a) shows the attenuation for a perfect structure, b) shows the attenuation for a structure with a defect. From reference [33].

potential variations result in wider band gaps. The dependence of the gap width on the dielectric contrast for a 2-D triangular lattice is shown in Figure 6. This figure also shows the optimal ratio of the hole radius, r, to the lattice constant, a, which gives the largest band gap. From this figure it is obvious that a dielectric contrast of at least seven is required if any gap is to be seen in a 2-D PBG material with a triangular lattice. The dielectric contrast for Si and air is approximately twelve at a wavelength of 1.55μm which would result in a gap of 15% of the midgap frequency.

Working in collaboration with researchers under the direction of Prof. John Joannopolous at MIT, investigations into 1-D PBG material have been carried out and these structures have advantages over the 2-D structures. The structure (shown in Figure 7) consists of a waveguide made of a high index material (silicon in our case) on a low index substrate (SiO_2). Along the center of the waveguide holes are etched. The holes provide the periodic dielectric variation. The waveguide confines and guides the light through the PBG structure.

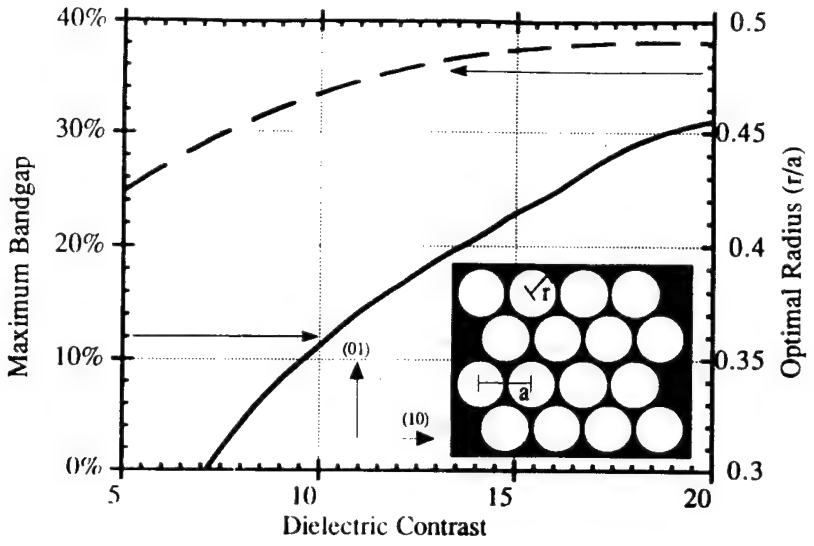

Figure 6: Dependence of band gap on dielectric constant for 2-D triangular lattice. Band gap is given as percent of center frequency. The optimal r/a ratio is also shown. From reference [38]

A single stretch of waveguide holes will act as a reflector over a large range of frequencies for guided modes. Removing one of the holes results in a defect mode in the range of reflected frequencies just as the 3-D case did. This missing hole will act as a microcavity. Unlike the 3-D case, the guided mode band gaps exist only for TE polarized light; any guided modes with TM polarization will not be reflected.

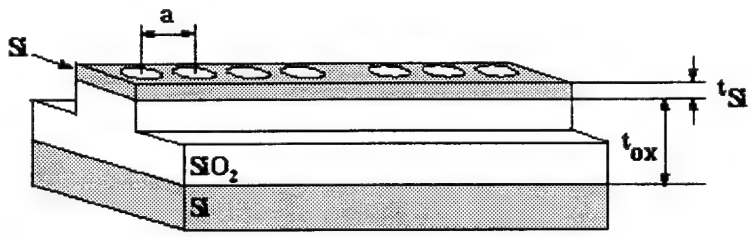

Figure 7: PBG material integrated into Si waveguide on SiO_2. The band gap scales with the period parameter, a. The value of 'a' is typically 0.3 times the mid-gap wavelength.

The waveguide integrated PBG structures have been analyzed theoretically [16, 17]. The Q for cavities consisting of single missing holes depends on the number of holes to either

side of the missing hole (see Figure 8). The PBG microcavities have small modal volumes. The modal volumes for these structures are estimated to be λ^3 which, from equation (2), results in enhancement factors as large as the cavity Q. The waveguide integrated PBG has the additional advantage of coupling the cavity output directly into a waveguide, eliminating the need for complicated coupling schemes.

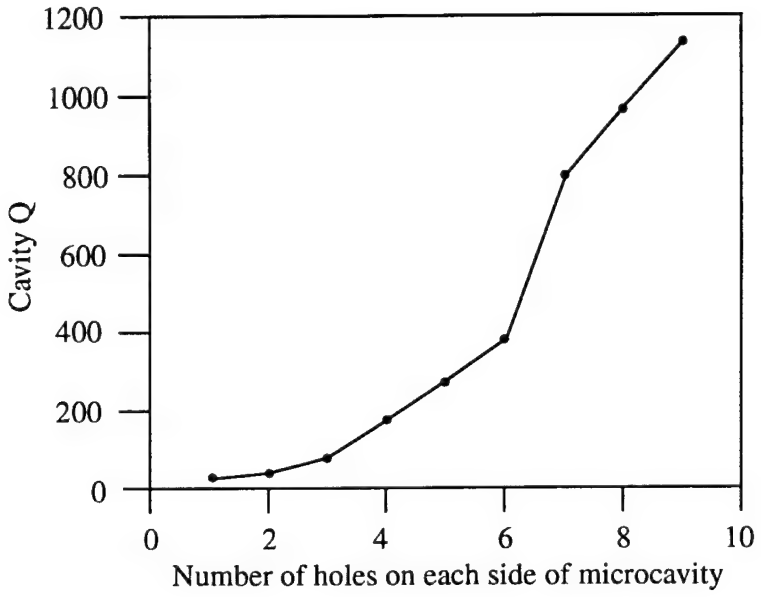

Figure 8: Cavity Q values as a function of the number of waveguide holes on either side of the cavity. From reference [17].

4 Research results

The goal of this research project is to evaluate the effects of enhanced spontaneous emission on Si:Er luminescence. The quality of the devices are highly dependent on material choices and processing. Additionally, the nature of resonances in waveguide integrated PBG structures and their material dependencies have never been investigated experimentally. The following sections detail the requirements for Si/SiO_2 confining structures and discuss the

Substrate	t_{Si} (μm)	t_{ox} (μm)	N_c (cm^{-3})	N_{def} (cm^{-2})
SIMOX	0.2	<0.45	10^{15}	10^5
BESOI	>1.0	>1.0	10^{18}	—
Unibond	0.2	>1.0	10^{15}	10^5
PolySi	0.2	>1.0	—	poly

Table 1: Summary of SOI technology capabilities as substrates for Si strip waveguides. t_{Si} is the Si thickness, t_{ox} is the oxide thickness, N_c is the carrier concentration, and N_{def} is the defect concentration.

different approaches for producing SOI material. Fabrication, evaluation and modelling of microdisk microcavities is presented. The development of PBG microcavities is discussed and the fabrication and analysis results are presented.

4.1 Silicon on insulator material

Both the microdisk and PBG microcavities take advantage of the development of Silicon-On-Insulator or SOI materials. These materials have been pursued to improve isolation between logic devices for integrated circuits, but have layer dimensions and refractive indices suitable for light confinement. The structures consist of a top silicon layer separated from on underlying silicon wafer substrate by a buried silicon dioxide layer. The important metrics for waveguide devices are the crystalline quality, thickness, and doping levels of the layers. The ability to control these parameters depends greatly on the processing techniques used. The major categories to be discussed here are SIMOX (Separation by IMplantion of Oxygen), wafer bonding, and polycrystalline silicon on oxide. Table 1 compares various the techniques and shows the defect levels and range of layer thicknesses possible. The development of polycrystalline silicon as a light guiding medium has been ongoing during the period of this work and results of the effort are included in this report.

The SIMOX technique begins with a standard silicon wafer into which oxygen is ion implanted. Implantation energies are typically 160keV with doses of $1.6x10^{18}cm^{-3}$. Following the implantation, a 1300°C, 6h anneal is performed to convert the implanted silicon into silicon dioxide and to anneal the implant damage from the upper silicon layer [42]. This is an excellent technique where thin top silicon layers are needed and oxide layers of 0.45μm or less are acceptable. The implantation damage can never be fully removed from the top silicon layer, and defect densities of $10^5/cm^2$ remain in the top layer. Additional problems include "pipes" of silicon that extend through the oxide and result from surface contamination [43]. The top silicon layer can be doped as desired or can remain nominally undoped, as is preferred for light propagation.

Wafer bonding technologies include BESOI (Bond and Etch-back Silicon On Insulator) and the Unibond process [44]. Bonds can be formed between oxide layers or between an oxide and a silicon layer simply by putting the surfaces in contact and heating them to 1100C. For bonding to occur requires that the surfaces be quite clean and defect free. BESOI and Unibond use different phenomenon to thin the top silicon layer. In BESOI, the top silicon wafer contains an etch-stop layer at the desired layer thickness. The entire silicon wafer behind this layer is etched off leaving a thin silicon layer. The remaining layer is always doped due to the etch-stop layer. The thickness of this layer is typically 1.0μm or more with variations in thickness of 10% common. The thickness and variation can be reduced with plasma thinning processes, but these are prohibitively expensive [45]. For the Unibond process, one of the wafers receives a high dose hydrogen implant prior to bonding. During the bonding process, voids form at the peak hydrogen concentration and the wafer cleaves

off. The surface is then chemical mechanically polished. Top silicon thicknesses of 2000$\AA$ are achievable with variations of 0.5%. The top silicon can remain nominally undoped. With either of the wafer bonding techniques, thick oxides are possible. Thermal oxides of 1.0μm or more are easily achieved.

Polycrystalline silicon on insulator material is under development as a light guiding material [46, 47]. The interest in polycrystalline silicon stems from its availability in standard silicon IC processing lines and the large range of silicon and oxide thicknesses possible. The drawbacks of the technology are the defective nature of the silicon due to grain boundaries. To form the structure, an oxide is formed either by thermal oxidation or by deposition. Polycrystalline silicon is then directly deposited, or amorphous silicon is deposited and then annealed into polycrystalline silicon. Annealed amorphous silicon has a much smoother surface, the deposited polycrystalline material typically has roughness measured to be 20nm. Because polycrystalline silicon is required if multilayer vertical cavities are to be achieved with the Si/SiO_2 material system, a program of assessing and limiting the losses of polycrystalline silicon has been undertaken. The next section details the work performed on polycrystalline silicon.

4.1.1 Polycrystalline silicon for light confinement

Reports of absorption in polycrystalline silicon indicated that the material would be unsuitable for light guiding. Absorption coefficients of 360dB/cm at λ= 1.54μm were reported [48]. We began using polySi as a prototyping material and found that the losses could be greatly reduced in a waveguide geometry. We deposited thick oxide (1.0 to 3.0μm) on a

Si wafer followed by 1.0μm thick polySi layers which were etched into straight waveguide sections. Loss measurements were performed by the cutback method and the results for different post-deposition treatments are shown in Figure 9.

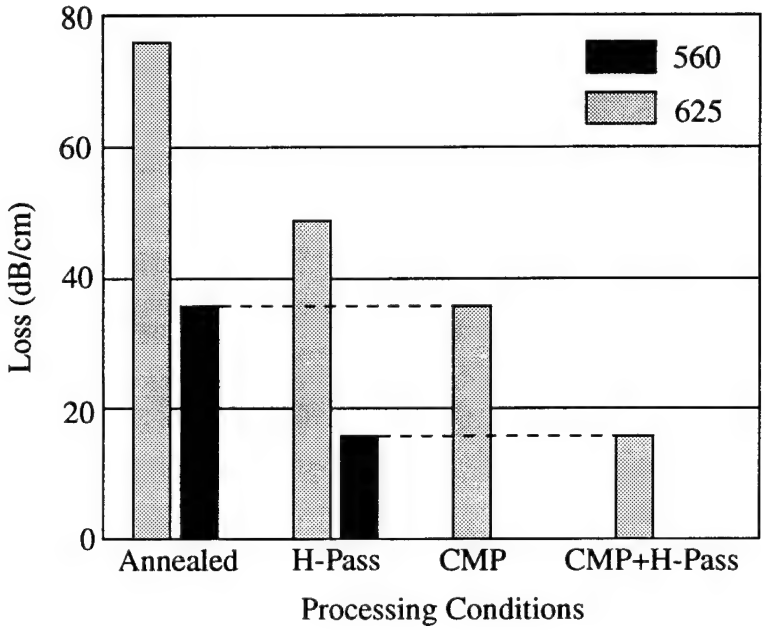

Figure 9: Optical loss in polycrystalline silicon at $\lambda = 1.54$ μm as a function of processing conditions.

The first measurements were made on polySi deposited at 625°C. Losses were found to be 75dB/cm. The deposited polySi is rough, with roughness measured by AFM to be 20nm rms. When this roughness is removed by chemical mechanical polishing (CMP), the loss is reduced to 35dB/cm. The improvement of 40dB/cm in attenuation is consistent with an analysis of roughness scattering [46].

To avoid the roughness and CMP step we deposit amorphous Si at 560°C and anneal at 600°C for 16 hours to convert the amorphous Si to polySi. The surface roughness of this polySi is typically 3nm rms, which is similar to the best results obtained by CMP. The loss in polySi waveguides prepared in this manner is 35dB/cm, consistent with the deposited

polySi waveguides treated with CMP. The remaining 35dB/cm is the bulk loss of the polySi.

The bulk loss can be further reduced by hydrogen passivation. Samples were subjected to a 300°C ECR hydrogen plasma for 60min. Following the hydrogenation, the residual waveguide loss is 15dB/cm. This represents the lowest loss ever acheived for polySi waveguides. The remaining loss is expected to be due either to an additional scattering mechanism at grain boundaries, perhaps due to band bending, or by incomplete passivation of defects.

With the reduced losses achieved in our polySi waveguides, the polySi/SiO_2 becomes an attractive system for prototyping before using expensive SOI substrates. PolySi also offers the opportunity to consider multiple levels of waveguides or layered structures such as distributed Bragg reflectors. Use of crystalline Si will reduce waveguide device loss appreciably, but losses associated with the fabrication are still of concern. The next section discusses the issue of fabrication induced loss.

4.1.2 Fabrication Induced Loss

The high index difference between Si and SiO_2 ($\Delta n = 2.0$) can lead to large roughness induced loss, as was seen in the case of the polySi waveguide measurements. This sensitivity to imperfection makes control of the etched waveguide features critical for maintaining low loss.

To assess the loss due to etched features, we fabricated waveguides using Unibond SOI substrates. The width of the waveguides varied from 8.0μm to 1.0μm in order to increase the interaction of the guided mode with the waveguide sidewall. The results of the waveguide loss as a function of the waveguide width are shown in Figure 10.

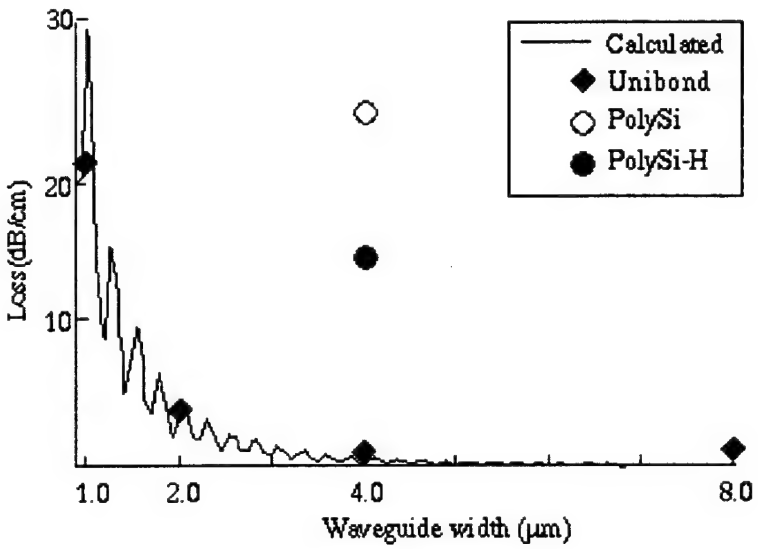

Figure 10: Measured loss of 0.2μm thick Unibond waveguides as a function of waveguide width. Solid line is calculated loss due to roughness.

For large waveguide widths ($\geq$4.0μm), the guided mode does not interact strongly with the sidewalls and the measured loss can be considered the bulk loss in the material. For both 4.0 and 8.0μm waveguides, this loss is measured to be near 1.0dB/cm. As the waveguide width decreases, loss due to sidewall roughness starts to increase. At 1.0μm width, we measure approximately 20dB/cm. Included with the measured data is a calculation of the loss due to roughness [49]. This loss is calculated by assuming that the waveguide has a perfectly periodic grating on the side that couples the guided mode to radiation modes. The oscillations in the calculated data are a result of the periodicity on the assumed grating. The trend of loss with width from the calculations matches well the measured data. For the calculation, a roughness of 15nm rms was used. Loss due to roughness depends on the square of the roughness; improved sidewall quality can greatly improve the waveguide performance. The microdisk devices are not greatly affected by the sidewall quality unless the disk radius is less than 1.0μm, for PBG devices with waveguide widths of 0.55μm, controlling the roughness

is critical. Experimental results for the microcavities are presented in the following sections.

4.2 Microdisk fabrication and test

Microdisk microcavities were investigated because of their simplicity and suitability to the Si/SiO_2 material system. Microdisks were fabricated from both SIMOX (separation by implantation of oxygen) and BESOI (bond and etch back) SOI substrates. The SOI substrates were doped with erbium using ion implantation. Ion beam energies of 360keV are used with doses of $10^{13}cm^{-2}$ to achieve peak erbium concentrations of $5x10^{17}cm^{-3}$. The substrates must then be annealed at 800°C for 30min to activate the erbium and to repair the implant damage. Critical parameters for the microdisk fabrication include mask generation and process flow. These will be discussed in the following section. Testing was performed using both photoluminescence and cathodoluminescence and the results are presented.

4.2.1 Microdisk processing

Writing small circular features accurately is difficult using optical pattern generators. The pattern generators break each circle into an overlapping series of rectangles. In order to acheive faithful reproduction of a circular feature, at least 48 such rectangles per circle are typically used. Because optical pattern generation overlaps these rectangles, the center of the circular feature can be overexposed and the outer edge of the circle can be underexposed. Patterns formed this way can be highly irregular in geometry. To avoid this problem, laser written or e-beam masks must be used. The pattern generators for these two types of mask writing technologies break the circular pattern into a rastered grid. One only needs to ensure

that the grid is fine enough not to be below the resolution of the exposure system being used for photolithography.

Testing with photoluminescence required that we use large arrays of microdisks that could be tested simultaneously. In order to achieve a detectable signal level, we wanted to have at least one tenth of the active volume of an unpatterned substrate. Additionally, we wanted the disks to be far enough apart so that they would not couple and alter the mode placement. We developed two masks, the first with large spacing between the disks to limit coupling. The second mask used a disk spacing of 5 times the tunnelling distance as defined by Slusher, and fractional volumes of 0.14 were achieved. There is a software limited tradeoff here between spacing and memory required for the mask data. While we could conceivably move the disks even closer, it would limit the number of disks we could use. The disk arrays are typically 1.0mm X 1.0mm and can contain as many as 100,000 disks per array.

The preferred process is to have the Er-related processing complete before patterning. The SOI substrates are implanted with erbium and oxygen and annealed at 800°C for 30min in nitrogen. Remnant implant damage can affect pattern transfer, resulting in a rough microdisk edge. Following the anneal, patterning and etching of the microdisk are performed. We used an SF_6 plasma etch to etch through the entire Si layer. In some cases we followed this with a buffered oxide etch to partially remove the oxide from underneath the disk. We did this to limit the coupling of the optical mode to the substrate. Figure 11 shows the result of the microdisk processing with a buffered oxide etch. Following the processing, the microdisks are ready for testing. Both photoluminescence and cathodoluminesence were performed on the microdisks and the results are presented in the following section.

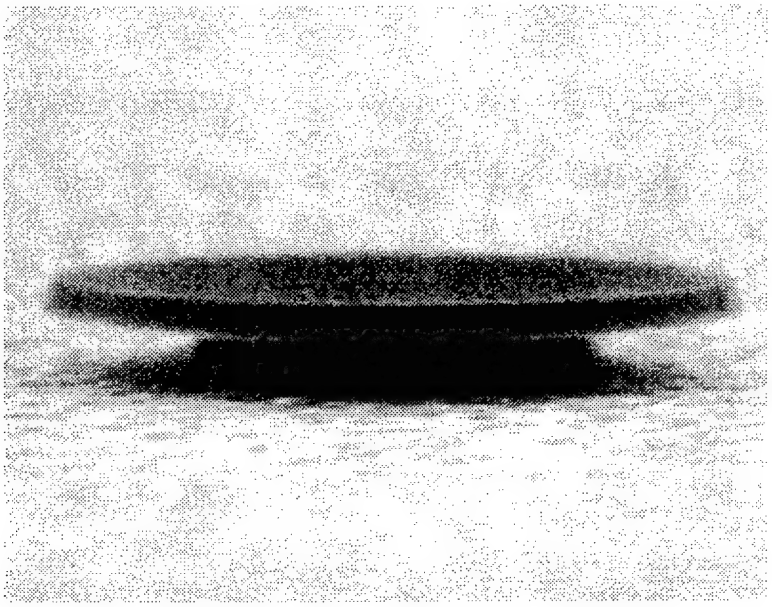

Figure 11: Si:Er microdisk fabricated from SIMOX material. Si etched in SF_6 plasma, oxide undercutting performed with buffered oxide etch. This disk is 0.2μm thick with a radius of $\approx$2.0μm.

4.2.2 Microdisk testing

Both photoluminescence (PL) and cathodoluminescence (CL) testing were performed on the microdisks. The PL measurements allow a larger active volume of Si:Er to be excited, while the CL measurements offer the possibility of testing individual disks.

Photoluminescence tests were performed on the microdisks. Sections of wafer with microdisks of only a single diameter were illuminated with an argon ion laser and the spectrum was determined with a spectrometer. The light detected is scattered out of the surface and the edges of the microdisk due to imperfections and also light that tunnels from the disk edge. In all cases, independent of the microdisk radius, the scattered light intensity was below the sensitivity of the measuring equipment (a liquid helium cooled Ge detector). This indicates that either the active volume of the disks is too small to show luminescence or that the microcavity is off-resonance and is not allowing light emission.

Cathodoluminescence (CL) measurements were performed on individual disks. The microdisk was scanned with a 40keV electron beam. The electron beam creates electron hole pairs in the silicon which can recombine and transfer their energy to the Er. The resulting Er luminesence is collected and detected by a liquid nitrogen cooled Ge detector. The luminesence passes through a notch filter centered at λ=1.54μm so that only Er related luminesence is detected. Using this technique we were able to map the resulting 1.54μm luminescence from a microdisk. Figure 12 shows the results. The microdisk shows greater luminescence intensity from the post area than from the edge of the disk. This is contrary to expectations for a whispering gallery mode with the light intensity being greatest at the disk edge. The radiation pattern we see can be attributed to the post actually optically pumping the disk. Si rich SiO_2 films have been shown to emit blue light under the appropriate excitation conditions. This emission can generate additional electron-hole pairs in the Si leading to greater 1.54μm emission. We measured the luminescence of the SiO_2 with the upper silicon layer removed and indeed found blue emission. The CL results for the SIMOX buried oxide are shown in Figure 13.

4.2.3 Microdisk analysis and conclusions

Microdisk testing is difficult because a null result (no measured signal) does not imply a poorly operating microdisk. In order to see microcavity effects it is necessary to overlap the spectrum of the Er luminescence with the microdisk mode. The mode position in wavelength is sensitively dependent on the disk radius and thickness. Figure 14a and b show these dependencies explicitly. The Si:Er spectra is shown plotted with the mode position as a

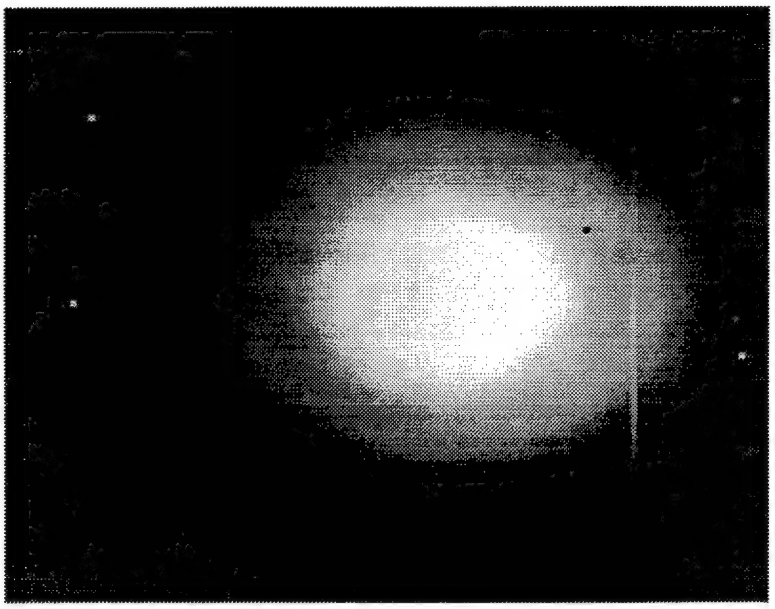

Figure 12: Map of $\lambda = 1.54\mu$m cathodoluminescence from Si:Er microdisk. Lighter colors correspond to higher intensity output.

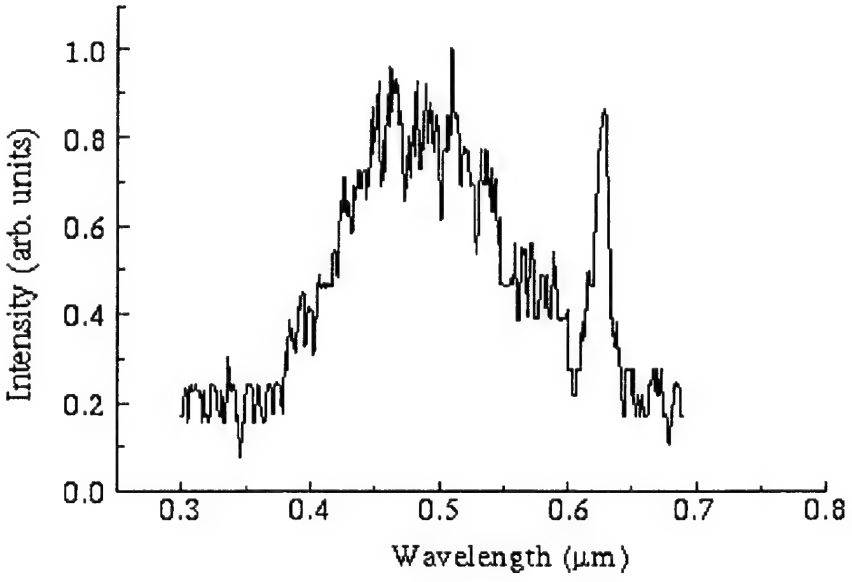

Figure 13: Cathodoluminescence of SIMOX buried oxide.

function of disk radius in Figure 14a. The mode position was calculated from the analysis published by Slusher [25]. It can be seen that small variations in disk radius can move the mode off of the maximum Er peak. Figure 14b shows the same type of dependence on disk thickness. If the thickness and radius are not controlled adequately, the microdisk mode will not overlap the Er luminescence and the spontaneous emission will actually be inhibited instead of enhanced. The mode positions are calculated using the approach by Slusher. It is not possible to predict the appropriate thickness and radius for modal overlap prior to fabrication because effective index calculations for these structures are only approximate and the uncertainty in measurement of the thickness and radius is larger than the acceptable tolerances.

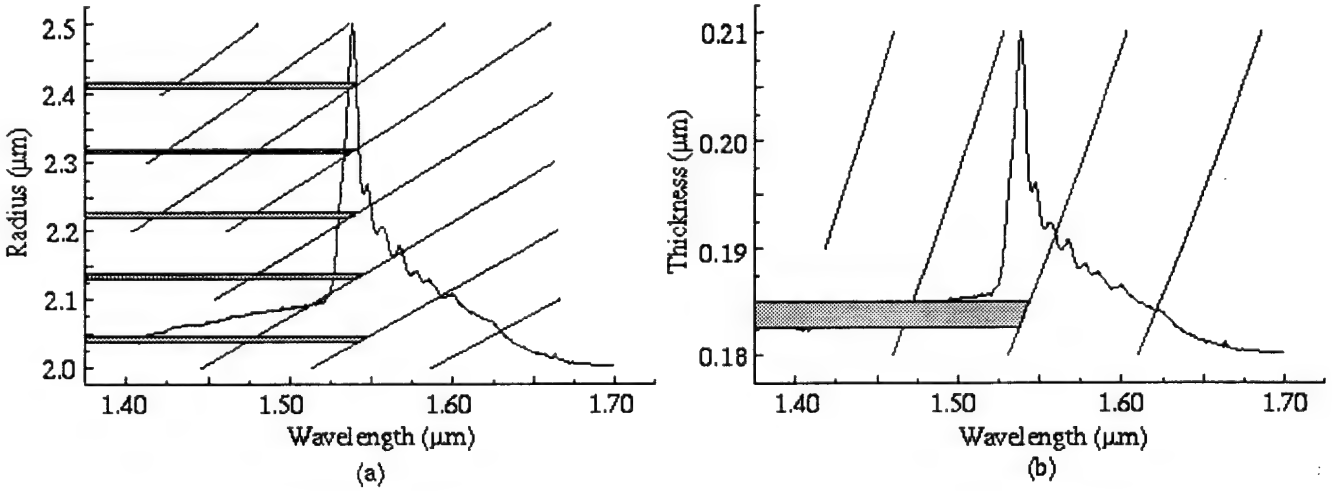

Figure 14: Dependence of microdisk mode position and typical Si:Er photoluminesence spectra. (a) mode position as a function of disk radius, (b) mode position as a function of disk thickness. Shaded areas show acceptable dimensions for disk mode overlap with maximum peak of Si:Er emission.

To surmount this problem, it is necessary to be able to measure the mode position without relying on the Si:Er luminescence. This measurement is possible if the microdisk is coupled to a waveguide. This basic structure is shown in Figure 15a. The disk is placed

in close proximity (approximately 0.2μm) to both waveguides. Light that is resonant in the microdisk will couple from the input waveguide to the output waveguide. A calculation of the transmission at the output of guide 2 is shown in Figure 15b. It should be noted that the resonant peaks here are all double moded. The double lobes are due to the existence of modes coupling across the disk. Measurements of the filter characteristics of the waveguide coupled disk would provide a diagnostic for determining the appropriate disk radius for emission enhancement.

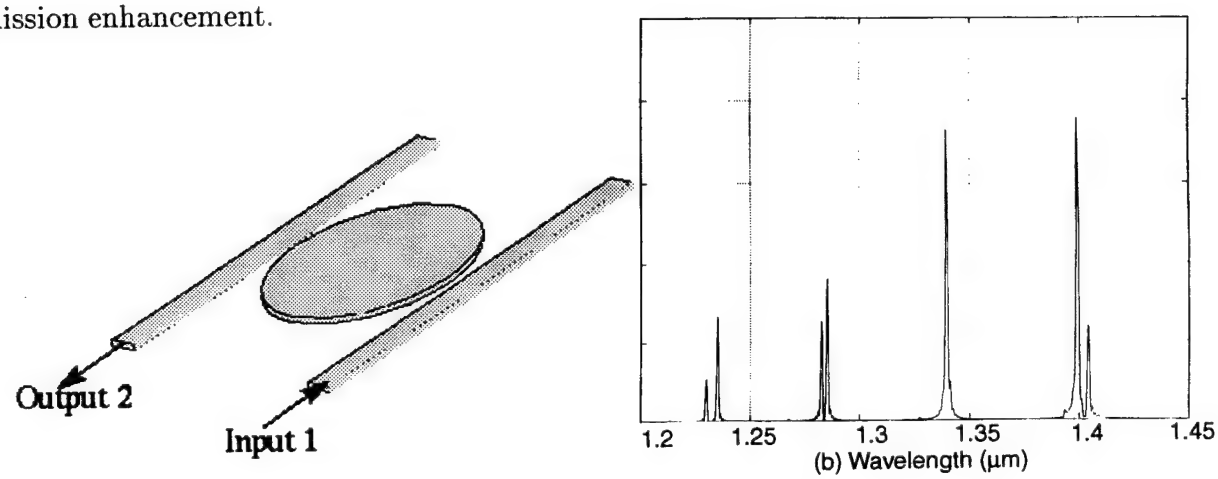

Figure 15: Waveguide coupled microdisk device. (a) device schematic, (b) output of waveguide 2 with broadband input to waveguide 1.

Because the microdisk acts as a filter, it can be considered for wavelength division multiplexing applications. In this configuration a disk radius is chosen to drop a specific wavelength from one waveguide bus to another. An additional possibility is to couple multiple disks to a single waveguide. This configuration could provide a compact amplification medium for Si:Er laser design. This type of amplification section can greatly reduce the required waveguide length for net gain as the disk modes effectively increase the path length due their high Qs.

The approach we have taken with the microdisks allowed us to understand the difficulties

of testing an optically active material with small active volume. The conclusions generated here provide a more complete understanding of the microdisk system for future iterations. Many of the issues of the waveguide integrated microdisk, including how to fabricate and test such a structure, have been answered by our work with PBG microcavities. The results from these waveguide integrated structures are detailed in the following sections.

4.3 Photonic band gap fabrication and test

Our work with PBG structures covers two wavelength regimes: $\lambda = 5.0\mu$m and $\lambda = 1.54\mu$m. The longer wavelength devices have dimensions compatible with standard optical lithography and are produced in the Integrated Circuit Laboratory (ICL) at MIT. Devices with band gaps centered at $\lambda = 1.54\mu$m have minimum feature sizes $\approx 0.10\mu$m and require the use of e-beam and x-ray lithography available in the MIT Nanostrucures Laboratory (NSL). The testing of the structures was performed at $\lambda = 1.54\mu$m as a waveguide test set-up at this wavelength was readily available. The fabrication and test results from the 5.0μm and 1.54μm devices are presented in the next sections.

4.3.1 Fabrication of PBG's for λ=5.0μm

We fabricated PBG structures for use at 5.0μm. These devices consist of a single mode Si waveguide with a periodic series of holes etched through the waveguide. Fabrication of PBG structures for use at 5.0μm can be accomplished using standard optical photolithography. The hole radii for these structures are approximately 1.0μm with center-to-center distances of 2.0μm and waveguide widths of approximately 2.2μm. The predicted band gap for these

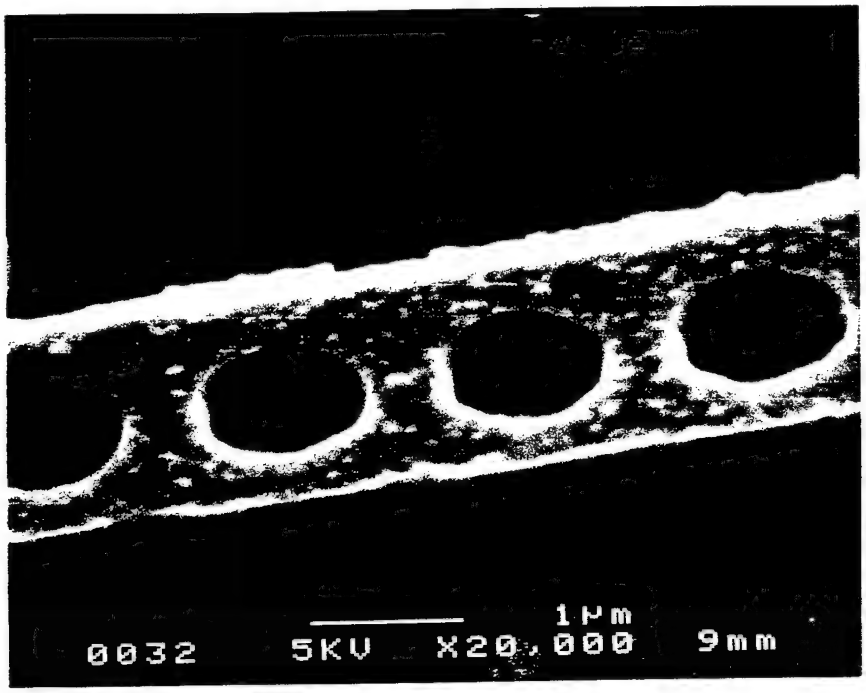

Figure 16: PBG structure in polySi waveguide. PBG device has band gap centered at λ=5.0μm. Hole radius is 1.0μm, waveguide width is 2.25μm, hole spacing is 2.0μm. Device fabricated using optical lithography.

structures is 20% of the center frequency for TE modes. The silicon thickness for single mode operation is $\approx$4000$\mathring{A}$. An important consideration for these structures is the buried oxide thickness. A thick oxide is always desired to keep losses due to leakage to the underlying silicon low. At λ = 5.0μm the required oxide thickness to keep losses limited to 1dB/cm is 3.0μm.

Because of the thick oxide and thin silicon layer needed for these devices, we chose to used deposited oxide and polySi as starting materials. An optically generated mask was used to pattern the substrates. The minimum feature size of the structure is 0.50μm, which represents the limit of the exposure source, a 408nm mercury lamp. The polySi is etched in an SF_6 plasma. The results of the processing are shown in Figure 16.

We fabricated a number of waveguides on a single sample, varying only the number of holes in each guide. No microcavity structures were included on this mask. The theoretical

band gap for this structure spans from 4.8μm to 5.2μm. At this point we don't have a source which can span this wavelength range, and the optics for coupling into small structures at these wavelengths are not widely available. We proceeded to probe these structures with 1.54μm excitation and the results follow.

4.3.2 Testing of $\lambda = 5.0\mu$m PBG structures

We used an existing waveguide test set-up to evaluate the $\lambda = 5.0\mu$m PBG devices. The test bench is shown in Figure 17. The source in this set-up is a $\lambda = 1.54\mu$m superluminescent diode. The diode is coupled into a single mode fiber with a conical tip, which is used to butt-couple into a polished waveguide facet. The fiber tip is mounted on a three axis translation stage with piezo-electric position control. The sample mount also has three axis translation as well as three axis rotation. Light exiting the waveguide can be imaged onto a camera or photodetector. Additionally, light scattered from the surface of the waveguide can be imaged and detected.

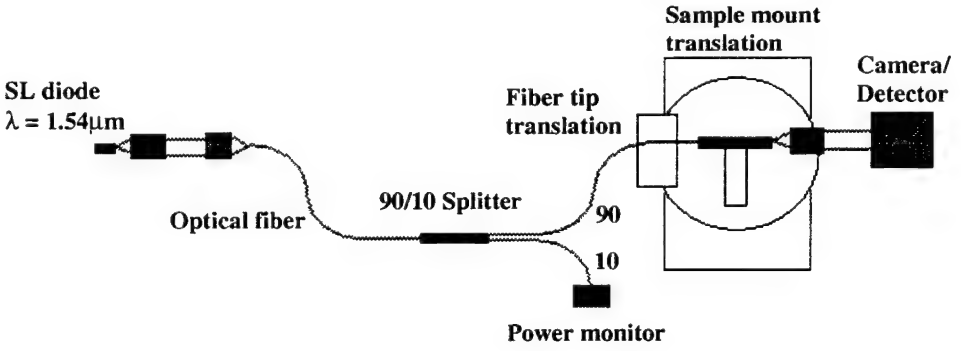

Figure 17: Waveguide test bench for $\lambda = 1.55\mu$m testing.

At $\lambda = 1.54\mu$m the 5.0μm PBG structures are expected to radiate this wavelength. The radiation occurs due to the periodicity of the PBG structure. The periodicity essentially

folds the guided modes of the waveguide into the radiation modes (similar to band folding in semiconductor systems). The PBG structure can then act as an input and output coupler for the waveguide. This PBG coupler is similar to a grating coupler, however the PBG coupler is much more compact (5.0μm compared to 200μm). The PBG coupler differs from the grating coupler in that the output is not angularly dependent. We have been able to couple into and out of the PBG holes . Figure 18 shows the PBG acting as an output coupler. Light is incident on the waveguide from the left (the large splotch of light is a reflection back onto the fiber tip). This light propagates down the waveguide to the PBG structure. Because the waveguide is composed of polySi deposited at 625°C with no CMP, the surface is rough and the scattered light from the roughness is evident down the length of the guide. At the PBG section (4 holes in this case) a large bright spot is seen. This intense spot is the output light from the PBG structure. We have also performed the reverse operation. The optical fiber was aligned to the holes in the waveguide and light coupled into the waveguide mode was detected at the waveguide output.

The output coupled power as a function of the number of holes is plotted in Figure 19. It can be seen that the effect saturates with only 4 holes; adding more holes does not improve the output coupling, giving evidence that the PBG works on small length scales and requires only a few periods for operation.

The $\lambda = 5.0\mu$m PBG work is continuing and a test bench for evaluating these structures at $\lambda = 5.0\mu$m is under construction. The testing at $\lambda = 1.54\mu$m is much easier, however the processing of devices for this wavelength range required considerable development. The results of this development are discussed in the next section.

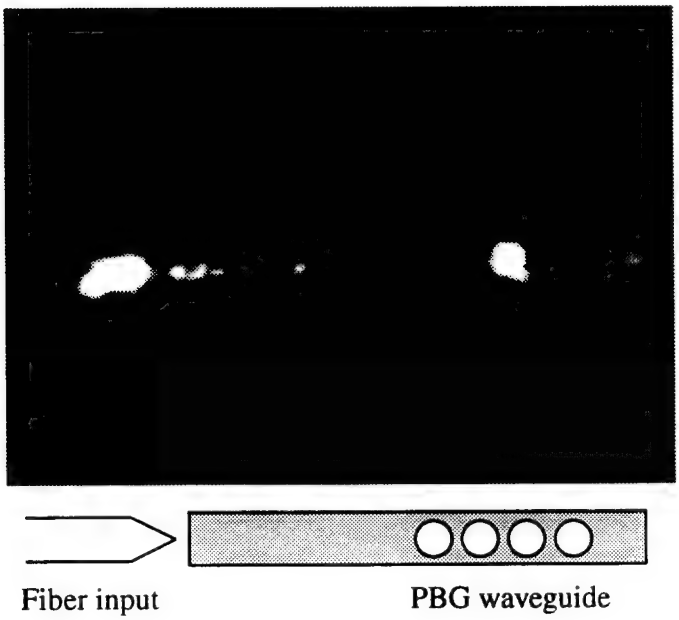

Figure 18: Scattered light and light output from a 5.0μm PBG structure. Input light is at $\lambda = 1.54\mu$m. The light is incident from the left.

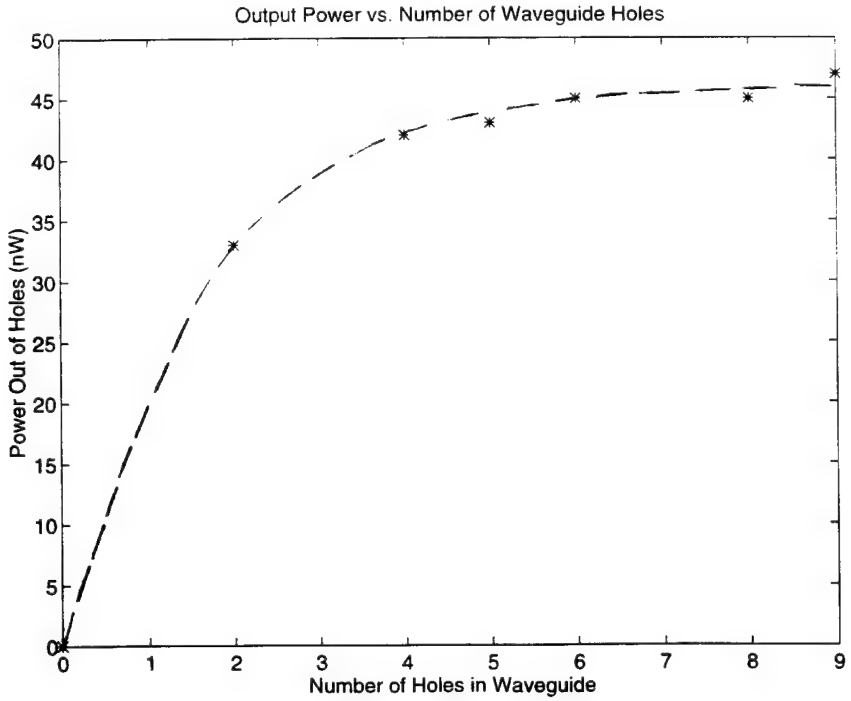

Figure 19: Scattered λ=1.54μm light measured from a PBG structure with band gap at 5.0μm as a function of the number of holes in the PBG structure.

4.3.3 Fabrication of PBG's for λ=1.54μm

The dimensions of PBG devices scale with the wavelength. Moving from 5.0μm to 1.54μm reduces the minimum feature size to $\approx$0.10μm. This dimension is not resolvable with standard optical lithography. Either direct write e-beam or x-ray lithography is necessary to accurately pattern PBG devices compatible with Si:Er. We chose to use x-ray lithography because many processing runs could be completed with a single mask. The ability to run multiple runs is important as e-beam writing times for the devices are long (typically an entire day). We performed the x-ray processing in the Nano-Structures Laboratory (NSL) of Prof. H. I. Smith at MIT. Much of the processing reported here directly stems from work developed in the NSL.

The first step in x-ray lithography is the creation of an x-ray mask. The completed mask consists of a thin silicon nitride membrane (typically 3.0μm thick) supported by a pyrex ring. The mask pattern is defined by 600$\AA$ gold on the silicon nitride. The gold provides about 10dB of absorption for incident x-rays.

The mask pattern definition requires a direct write e-beam onto the membrane followed by an electroplating step. The e-beam generates the pattern in PMMA that has been spun onto the membrane (the PMMA thickness is typically 2500$\AA$). The PMMA is then developed. The resulting features are then filled with 600$\AA$ of gold by electroplating. A thin layer of metallization on the silicon nitride provides the contact for the electroplating, but does not appreciably attenuate the x-ray signal.

There are several e-beam writing related considerations that can affect device performance. These include choosing a field size and controlling pattern stitching. The mask

pattern is broken into small fields which the e-beam system writes without translating the sample stage. This field size determines the actual spot size of the e-beam and impacts the available resolution for pattern definition. We typically choose the field size so that the period of the PBG structure is an integer number of e-beam pixels (or spot sizes). Choosing the field size in this manner allows accurate control of this critical parameter. For the devices we are considering, field sizes of $\approx 125\mu$m are used, resulting in pixel sizes of $\approx$7.0nm.

Because the field size is smaller than the ultimate waveguide length (typically 2.0mm), the sample stage must be translated a number of times in order to write a complete waveguide. The translation of the sample stage can result in misalignment between adjacent fields. This shift between fields is known as a field stitching error. While the affects of field stitching errors on device performance are not known, we took measures to avoid them as much as possible. This requires control of the translation system as well as stability of the e-beam column.

The e-beam written mask is the wrong polarity for pattern transfer to a substrate. This mask acts as a "mother" and is used to produce "daughter" masks used in the substrate patterning. Using this approach always allows a copy to be made without needing to perform an additional e-beam writing step. The delicacy of the silicon nitride membranes make them susceptible to breakage and retaining the mother mask is crucial to avoid processing delays.

The daughter mask is made by bringing the mother mask into close proximity to an x-ray mask blank. The spacing between the masks is typically maintained at 3.0μm by Al studs which are evaporated onto the daughter mask. PMMA on the daughter mask is exposed to x-ray radiation through the mother mask and the pattern is transferred. The daughter

mask is then developed and electroplated to form the correct polarity mask for transfer to a substrate.

Transfer of the pattern to the substrate is similar to the daughtering process. The sample, coated with PMMA, is brought into proximity with the daughter mask and exposed with x-rays. The typical exposure times are 5-7hours. This rather long exposure time is a result of the limited sensitivity of the PMMA to the x-ray radiation. The PMMA as then developed and a thin layer, $\approx 500\mathring{A}$, of Cr is e-beam evaporated onto the sample. Lift-off of the Cr is performed by soaking the sample in acetone and dissolving the PMMA. The result is a Cr mask directly on the substrate. The lift-off process is used as the PMMA can not stand up to the subsequent plasma etching.

Two etch steps are performed on the SOI substrates. The first etch is a plasma of CF_4 with $15\%O_2$ silicon etch. The top layer of Si is completely etched through; this step typically takes about 12minutes. The next step is an etch into 0.30μm of the underlying oxide. CHF_3 is used for this etch step. Following the etching, the Cr is removed with a wet etch. The sample is then diced with a die saw and polished in preparation for testing. A typical result from the processing is shown in Figure 19. This particular structure was processed in Unibond SOI material. The top Si layer is 0.20μm and the underlying SiO_2 is 1.0μm thick.

Each waveguide on the mask has input and output flares used to improve input and output coupling to these submicron waveguides. The flares widen the waveguide to 5.0μm at the input and output. The structures on a single die include 10 straight waveguides for references, PBG structures with no microcavities, PBG structures with cavities, and PBG coupling structures. For the PBG structures without microcavities, the number of holes in

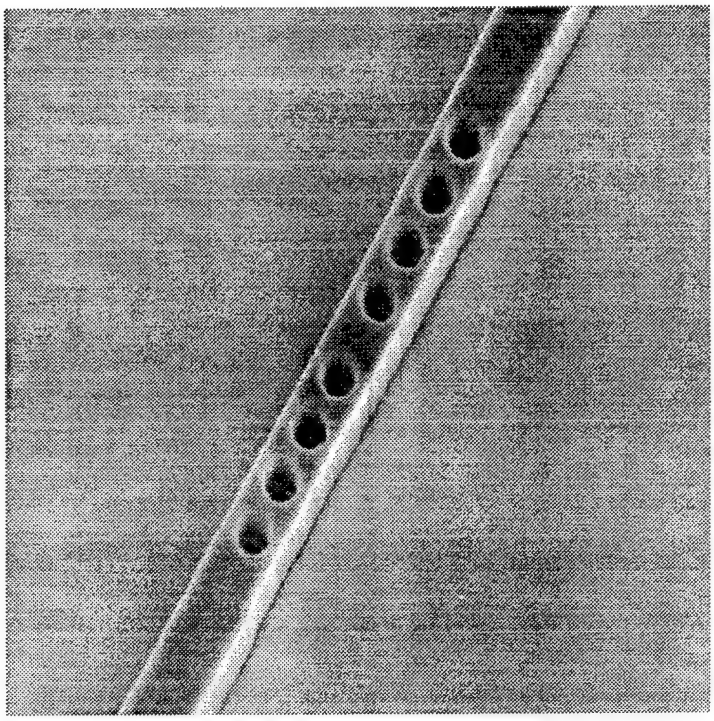

Figure 20: PBG microcavity for λ=1.54μm. Device processed using x-ray lithography. Hole diameter is 0.30μm, waveguide width is 0.50μm, and hole spacing is 0.48μm.

the waveguide is varied from two to six. The microcavity resonance position is varied by changing the length of the "defect" in the PBG structure (the distance between the two sets of four holes shown in Figure 19). The coupling structures are PBG devices with every-other hole removed. This essentially folds the Brillouin zone for the PBG device and couples a guided mode into radiation modes.

To assess the operation of the PBG structures, we needed to perform spectroscopy on the devices. The next section details our work on experimentally assessing the function of the PBG waveguides.

4.3.4 Characterization of PBG's at λ=1.54μm

The calculated transmission of the λ=1.54μm PBG structure is shown in Figure 20. We use

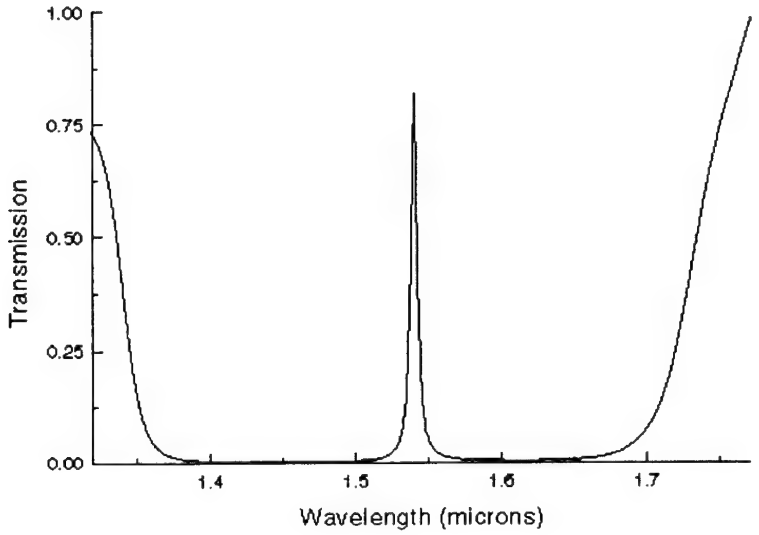

Figure 21: Calculated transmission for the 1-D PBG structure with resonance designed for λ=1.54μm.

coupling approaches similar to that of the λ=5.0μm PBG testing in order to evaluate the operation of the λ=1.54μm PBG devices. To look at the spectrally dependent features of the devices, we use a broadband Er-doped fiber laser (EFL) made available to us by Prof. Erich Ippen. This laser has a usable bandwidth of approximately 80nm. This source was coupled into a waveguide and the spectrum at the output of the waveguide was measured using an optical spectrum analyzer. Figure 21 shows the spectrum of the EFL.

To evaluate the repeatability of the measurements, we performed spectroscopy on Unibond waveguides of widths ranging from 8.0μm down to 1.0μm. Several measurements were performed on a single waveguide in order to evaluate repeatability and sensitivity to small changes in alignment. Figure 22 shows three measurements of the same 1.0μm waveguide. The data here has been normalized to the spectrum of the Er-doped fiber laser and as well has been normalized so that the peak of the transmission is 1.0. The repeatability was found

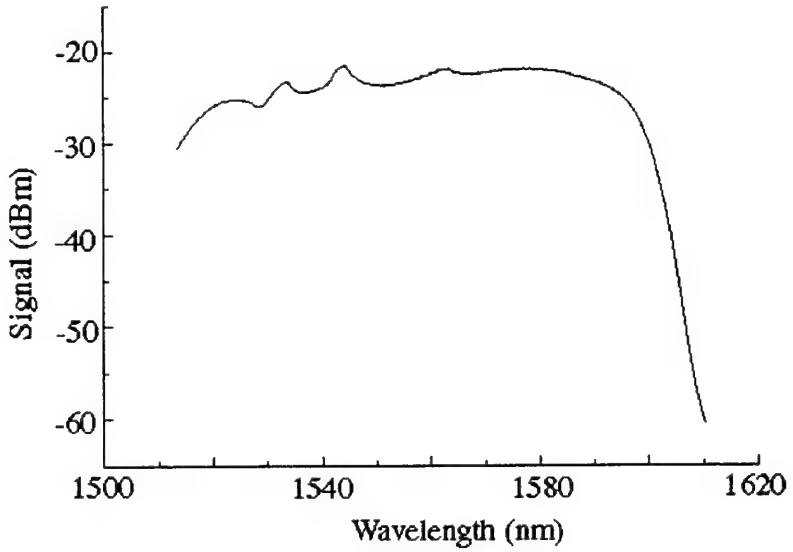

Figure 22: Spectrum of the Er-doped fiber laser used for PBG device evaluation at $\lambda = 1.54\mu$m.

to be quite good (less than 3

The PBG waveguides had too little signal at the output for spectroscopy to be performed. The high loss of these waveguides is attributed to sidewall roughness as demonstrated in the section on fabrication induced loss presented earlier. In order to be able to measure the bandgap and resonance in the waveguide integrated PBG, we estimate that we need a factor of ten improvement in signal to noise ratio. This can be achieved by improving the coupling of the EFL to the fiber that transports the light to the waveguide. The EFL was measured to have 40mW total power. The power measured at the waveguide was only 1mW. It should be possible to couple 50% of the available power into the fiber optic and this will provide the additional signal required. The actual cavity length is small, so sidewall roughness should not adversely affect the resonance properties even if the waveguide is quite lossy.

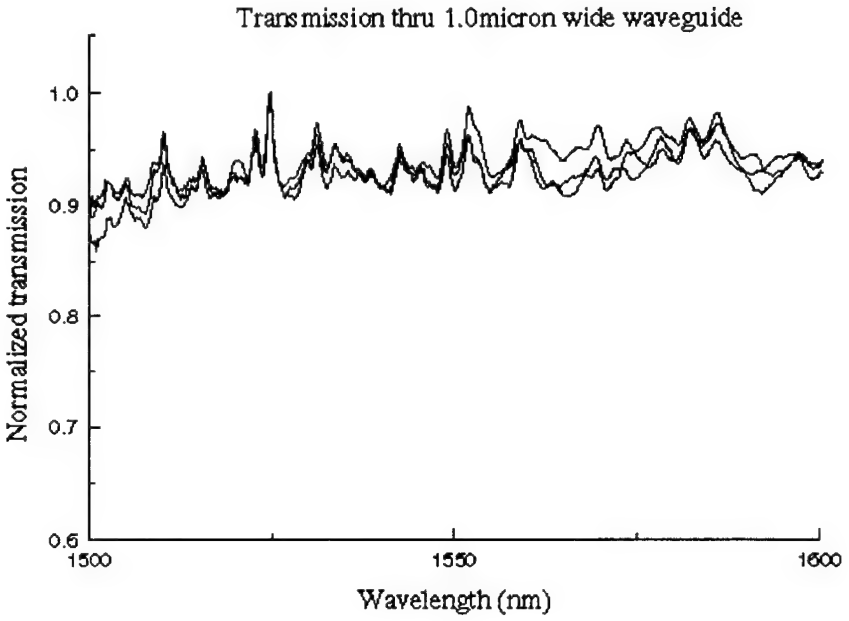

Figure 23: Normalized transmission as a function of wavelength for 0.2x1.0μm Unibond waveguide.

4.3.5 PBG microcavity analysis and conclusions

We have successfully fabricated 1-D PBG structures at both 5.0 and 1.54μm. A test facility for the 1.54μm devices has been established and preliminary spectroscopy measurements at these wavelengths have been performed. There are some concerns regarding whether we can overlap the available spectrum of the EFL with the resonant mode in the PBG microcavity. To this end, we have tried to include a number of "tuned" structures on the x-ray mask to ensure that we will find an appropriate device. The resonance frequency can be tuned either by changing the microcavity dimensions (the longer the cavity is, the longer the wavelength of the resonance) or by scaling the dimensions of the entire PBG structure. In our case, we opted to change the microcavity length.

The performance of the PBG microcavity is critically dependent on dimensions and is

especially dependent on the waveguide thickness. For example, a 10% variation in thickness, keeping all other parameters the same, will cause the resonance to shift by 100nm and will limit the transmission on resonance to 65

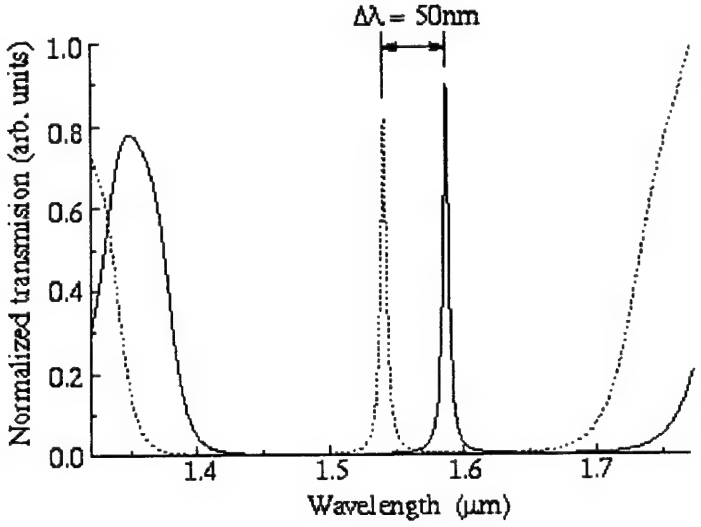

Figure 24: Effect of transmission on thickness variation. Resonance peak is shifted to longer wavelengths.

The 1-D PBG structures are particularly susceptible to radiation loss. The effective index of the waveguide with the holes etched is substantially lower than that of an unpatterned waveguide. The lowered effective index allows the mode to spread outside of the waveguide considerably. The spread can result in the loss of the resonant mode to the SOI substrate. The tendency for these structures to scatter can be seen from the band structure of the device shown in Figure 24. The separation between guided modes and radiation modes is shown by the hatched line. The band gap occurs between the first two guided modes. Because these modes are quite high in the Brillouin zone, the modes are close to the radiation modes. In order to reduce the coupling to radiation modes, it is necessary to increase the effective index in the PBG section. This is most easily accomplished by decreasing the hole radius.

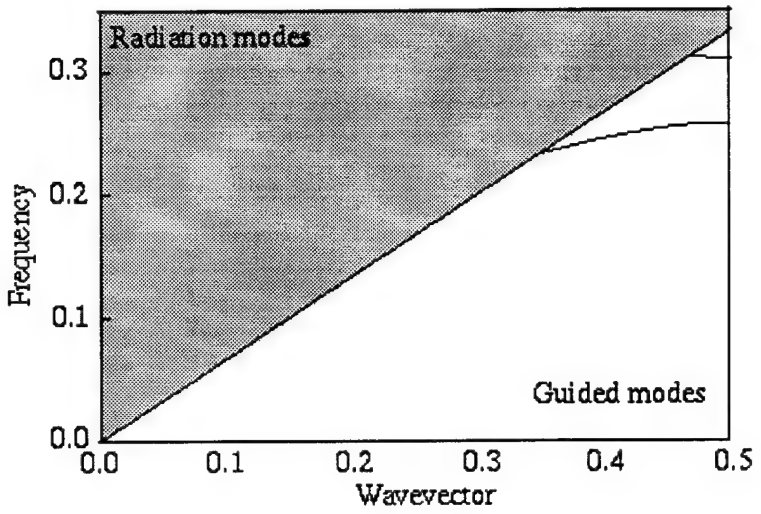

Figure 25: Band structure of 1-D PBG structure.

4.4 Alternative light emission schemes

All of the data in this report centered on using crystalline Si which has been implanted with Er. While this materials system has its advantages, there are several limitations that can be overcome by looking at alternative Si:Er technologies. Work in our laboratory has centered on the development of UHV-CVD grown Si and SiGe doped with Er and on Er-implanted polySi. The UHV-CVD work is a path to higher concentrations of optically active Er in Si. The polySi work allows the consideration of vertically integrated microcavities for evaluating spontaneous emission enhancement effects.

The UHV-CVD growth is performed in a reactor developed by the Kimerling Group at MIT. This growth chamber has been successful in depositing Si layers with as much as 10^{21}cm^{-3} Er. Selection of the Er precursor allows engineering of the ligand field surrounding the Er. To date the best results achieved from Si:Er from UHV-CVD are from material with 10^{19}cm^{-3} Er using an oxygen containing precursor. The photoluminescence spectrum from this material is shown in Figure 25. The UHV-CVD material luminescence is comparable to

that of the best implanted material, indicating that not all of the incorporated Er is optically active.

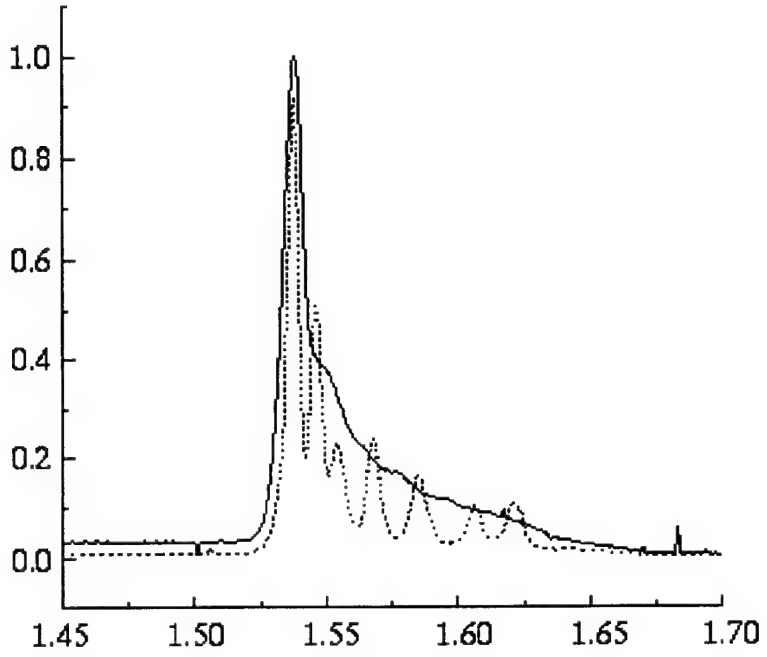

Figure 26: Photoluminescence spectrum of the UHV-CVD grown Si:Er at 4K (solid line) compared to implanted Si:Er (dashed line).

PolySi heavily doped with Er and O has been shown to emit strongly at 1.54μm. We are interested in determining whether we could see similar low temperature response from doped polySi that we see from crystalline Si. If the quenching mechanism is similar, we can use the polySi in microcavity devices and determine the effects of spontaneous emission enhancement in this material. We are currently measuring the dependence of the emission from this material as a function of annealing conditions following the implantation. Figure 26 shows the results of a 48hr anneal at 600°C followed by a 900°C rapid thermal anneal for 15s. The PL spectrum does not show the characteristic sharp line luminescence of Si:Er, therefore the microcavity dimensional tolerances are somewhat less constraining. Further

work will be done to optimize the performance of this material.

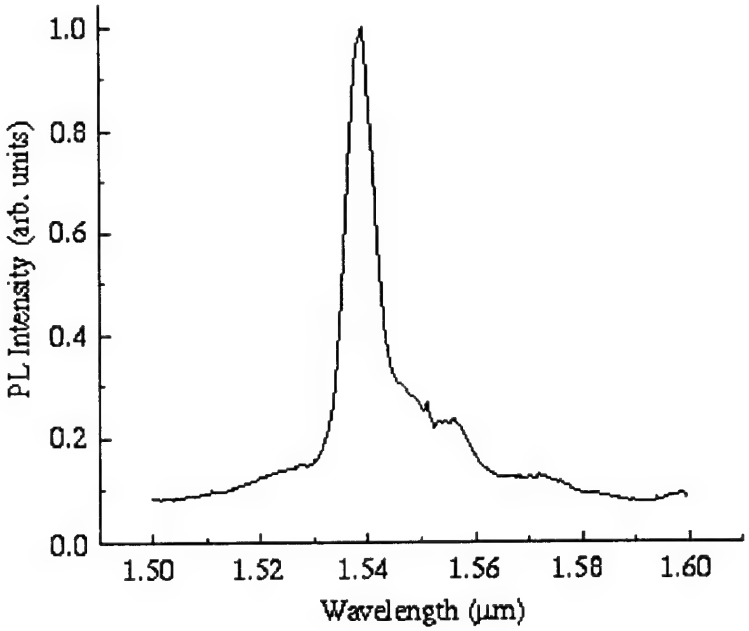

Figure 27: Photoluminescence spectra of Er-doped polycystalline Si.

5 Conclusion

We have demonstrated the development of two types of silicon-based microcavities for the control of spontaneous emission from Si:Er. The development of these microcavity devices has uncovered challenges for both materials and design. This summary section reviews the challenges and the solutions we have developed to meet the challenges.

The devices we have been discussing rely on SOI substrates. Of the available substrate technologies, only Unibond wafers are capable of meeting the stringent dimensional requirements for our microcavity devices, and none of the technologies are suitable for vertically integrated structures. We developed polycrystalline Si as an alternative SOI materials system. Optical losses at λ=1.54μm in polySi were initially measured to be 75dB/cm, and we

have reduced them to 15dB/cm. PolySi is a useful tool for prototyping as a large range of polySi and SiO_2 thicknesses are acheivable; polySi is available in most IC processing lines; and the layers are deposited, which allows the development of multilayer structures.

The large refractive index difference between silicon and air makes edge roughness a critical limitation to low loss transmission. Measurements of losses in crystalline Si strip waveguides as a function of strip width show that losses can be as high as 20dB/cm with waveguides 1.0μm wide. Calculations of the loss due to edge roughness show that this loss increases dramatically for waveguides with widths smaller than 1.0μm. These measurements show that, for devices coupled to single mode silicon waveguides, control of the etched walls is critical.

Microdisk microcavities were fabricated and evaluated using photoluminescence and cathodoluminescence testing. The PL testing was unable to detect any Si:Er signal. This result was correlated to the small active volume of the microdisks. CL testing allowed mapping of the 1.54μm emission from a single disk. An assessment of the fabrication tolerances of the microdisks shows that control of the radius and thickness are critical to the overlap of the resonant cavity mode with the peak of the Si:Er emission. To overcome this obstacle, it is proposed that microdisks be coupled to external waveguides in order to evaluate the mode positions before performing luminesence testing. The waveguide coupled microdisk configuration provides not only a predictive method of establishing mode position, but also a filter or coupler configuration for wavelength division multiplexing systems.

PBG devices were designed and fabricated for band gaps centered at λ=5.0μm and λ=1.54μm. The devices were evaluated at λ=1.54μm. The 5.0μm devices were fabricated

using standard optical lithography techniques and had a minimum feature size of 0.5μm. The devices, consisting of a series of periodic holes etched through a polySi waveguide were operated as input and output couplers at λ=1.54μm. These couplers are similar to grating couplers, but require only 10μm lengths as opposed to 250μm lengths for grating couplers. This shortened length relaxes constraints on pattern coherence and reduces the real estate required for the integrated device. Testing shows that only four PBG holes are required before the effect saturates, giving evidence that length scale required for acheiving PBG properties is small.

For PBG devices with a band gap at λ=1.54μm the minimum structural feature size is 0.10μm. To acheive this small dimension, we used a combination of e-beam and x-ray lithography for pattern transfer. This combination allowed us to fabricate 0.55μm wide waveguides with 0.30μm diameter holes etched through them. Calculations of the transmission through a resonant cavity consisting of two sets of three holes separated by a quarter of the hole period show 85% transmission on resonance. This resonant wavelength depends critically on the structure dimensions, and the use of e-beam and x-ray lithography allow excellent control of the device features. The critical structural parameter was found to be the device thickness. If the thickness varies 10% from the design thickness, the resonance shifts 50nm.

To test the PBG devices at 1.54μm we developed an experimental set-up using an erbium-doped fiber laser with an optical spectrum analyzer. The erbium-doped fiber laser has a usable spectrum from 1520 to 1600nm. To evaluate the set-up we coupled the light from the laser into a 1.0μm crystalline Si waveguide and measured the output spectrum. The measurement was found to be repeatible with an approximately 3% variation between scans.

Evaluation of the PBG waveguides was not possible as the signal to noise ratio at the output of these narrow waveguides did not provide a measurable signal. It is estimated that an additional factor of 10 in signal to noise ratio will be necessary to perform the measurements. This factor of 10 may be acheived by improving the coupling of the erbium-doped fiber laser to the waveguide, and by expanding the mode at the input of the waveguide in order to match the fiber mode more effectively.

The ability to test the effects of spontaneous emission in the microcavity devices is limited by the light output of the Si:Er material. Additionally, the narrow linewidth of the Si:Er luminescence reduces the tolerance to design and fabrication imperfections when compared to large gain bandwidth systems. To address these issues we are pursuing UHV-CVD grown Si:Er and polySi and amorphous Si implanted with Er. The UHV-CVD technique has provided samples with metastable incorporation of Er at concentrations of two orders of magnitude greater than implantation. Implantation into polySi and amorphous Si have been performed and the spectrum from these materials was found to be much broader than for implanted single crystal Si due to inhomogeneous broadening. These noncrystalline materials are expected to ease the dimensional constraints on the microcavity devices.

The research performed in this program, while primarily concerned with the development of microcavity devices in silicon, has opened areas of research which will allow the miniaturization of optical components in a materials system compatible with standard IC processing. Both the microdisk and PBG cavities, when coupled to waveguides, can act as filters, signal routers, and possibly compact gain sections for integrated laser devices. The use of a high index difference system such as Si/SiO_2 allows the reduction of waveguide dimensions to the

sub-micron range, and the associated optical componenents to square micron areas instead of square millimeter areas. The reduction in size allows higher densities of components to be integrated onto a single die. The device dimensions we are working with are more similar to those of integrated circuits in Si than to optical components in III-V, doped silica or other waveguiding systems, and may finally lead to an integrated optics technology that is not limited by yield or the reduced functionality of large devices.

References

[1] R. A. Modavis, D. G. Hall, J. Bevk, B. S. Freer, L. C. Feldman, B. E. Weir, *Isoelectronic bound exciton emission from Si-rich silicon-germanium alloys*, Appl. Phys. Lett. 57 (10), pp. 954, 1990.

[2] L. T. Canham, *Silicon quantum wire array fabrication by electrochemical and chemical dissolution of wafers*, Appl. Phys. Lett. 57 (10), pp. 1046, 1990.

[3] E. Werwa, A. A. Seraphin, L. A. Chiu, C. Zhou, and K. D. Kolenbrander, *Synthesis and processing of silicon nanocrystallites using a pulsed laser ablation supersonic expansion method*, Appl. Phys. Lett. 64 (14), pp. 1821, 1994.

[4] H. Ennen, G. Pomrenke, A. Axmann, K. Eisele, W. Haydl, J. Schneider, *1.54μm luminescence of erbium-implanted III-V semiconductors and silicon*, Appl. Phys. Lett., 43 (10), pp. 943, 1983.

[5] Y. G. F. Ren, J. Michel, Q. Sun-Paduano, B. Zheng, H. Kitagawa, D. C. Jacobson, J. M. Poate, L. C. Kimerling, *IC compatible processing of Si:Er for optoelectronics* in

"Rare Earth Doped Semiconductors" ed. by G. S. Pemrenke, P. B. Klein, and D. W. Langer, MRS Proc. Vol. 301 (Pittsburgh, PA, 1993).

[6] F. Priolo, G. Franzo, S. Coffa, A. Polman, V. Bellani, A. Carnera, C. Spinella, *Erbium implantation in silicon: a way towards Si-based optoelectronics* in "Rare Earth Doped Semiconductors" ed. by G. S. Pemrenke, P. B. Klein, and D. W. Langer, MRS Proc. Vol. 301 (Pittsburgh, PA, 1993).

[7] Y. G. F. Ren, *Erbium doped silicon as an optoelectronic semiconductor material*, PhD dissertation, MIT, 1994.

[8] J. Michel, J. L. Benton, R. F. Ferrante, D. C. Jacobson, D. J. Eaglesham, E. A. Fitzgerald, Y. -H. Xie, J. M. Poate, L. C. Kimerling, *Impurity enhancement of the 1.54μm Er^{3+} luminescence in silicon*, J. Appl. Phys., 70 (5), pp. 2672, 1991.

[9] D. Kleppner, *Inhibited spontaneous emission*, Phys. Rev. Lett. 47 (4), pp. 233, 1981.

[10] H. Yokoyama, K. Nishi, I. Anan, H. Yamada, S. D. Brorson, E. P. Ippen. *Enhanced spontaneous emission from GaAs quantum wells in monolithic microcavities*, Appl. Phys. Lett. 57 (26), pp. 2814, 1990.

[11] W. F. Schubert, A. M. Vredenberg, N. E. J. Hunt, Y. H. Wong, P. C. Becker, J. M. Poate, D. C. Jacobson, L. C. Feldman, G. J. Zydzik, *Giant enhancement of luminescence intensity in Er-doped Si/SiO_2 resonant cavities*, Appl. Phys. Lett. 61 (12), pp. 1381, 1992

[12] A. M. Vredenberg, N. E. J. Hunt, E. F. Schubert, D. C. Jacobson, J. M. Poate, G. J. Zydzik, *Controlled atomic spontaneous emission from Er^{3+} in a transparent Si/SiO_2 microcavity*, Phys. Rev. Lett., 71 (4), pp. 517, 1993.

[13] Y. Yamamoto, S. Machida, Y. Horikoshi, K. Igeta, *Enhanced and inhibited spontaneous emission of free excitons in GaAs quantum wells in a microcavity*, Opt. Comm. 80 (5,6), pp. 337, 1991.

[14] E. F. Schubert, Y. -H. Wang, A. Y. Cho, L. -W. Tu, G. J. Zydzik, *Resonant cavity light-emitting diode*, Appl. Phys. Lett. 60 (8), pp. 921, 1992.

[15] S. L. McCall, A. F. J. Levi, R. E. Slusher, S. J. Pearton, R. A. Logan, *Whispering-gallery mode microdisk lasers*, Appl. Phys. Lett. 60 (3), pp. 289, 1992.

[16] R. D. Meade, A. Devenyi, J. D. Joannopoulos, O. L. Alerhand, D. A. Smith, K. Kash, *Novel applications of photonic band gap materials: low-loss bends and high Q cavities*, MIT ILP Report, 3-61-94.

[17] J. N. Winn, *Dynamic studies of photonic crystals*, MS Thesis, MIT, 1994.

[18] S. Coffa, G. Franzo, F. Priolo, A. Polman, R. Serna, *Temperature dependence and quenching processes of the intra-4f luminescence of Er in crystalline Si*, to be published.

[19] H. Efeoglu, J. H. Evans, T. E. Jackman, B. Hamilton, D. C. Houghton, J. M. Langer, A. R. Peaker, D. Perovic, I. Poole, N. Ravel, P. Hemment, C. W. Chan, *Recombination processes in erbium-doped silicon*, Semicond. Sci. Technol., 8, pp. 236, 1993.

[20] A. J. Neuhalfen, B. W. Wessels, *Thermal quenching of Er^{3+}-related luminescence in $In_{1-x}Ga_xP$*, Appl. Phys. Lett., 60 (21), pp. 2657, 1992.

[21] S. Haroche, J. -M. Raimond, *Cavity quantum electrodynamics*, Sci. Amer., pp. 54, April 1993.

[22] H. Yokoyama, *Physics and device applications of optical microcavities*, Science 256, pp. 66, 1992.

[23] Y. Yamamoto, S. Machida, G. Bjork, *Micro-cavity semiconductor lasers with controlled spontaneous emission*, Opt. Quant. Elec., 24, pp. S215, 1992.

[24] Y. Yamamoto, R. E. Slusher, *Optical processes in microcavities*, Phys. Today, pp. 66, June 1993.

[25] R. E. Slusher, *Semiconductor microlasers and their applications*, Opt. Photon. News, pp. 8, February 1993.

[26] E. Yablonovitch, *Inhibited spontaneous emission in solid-state physics and electronics*, Phys. Rev. Lett., 58 (20), pp. 2059, 1987.

[27] H. Yokoyama, S. D. Brorson, *Rate equation analysis of microcavity lasers*, J. Appl. Phys., 66 (10), pp. 4801, 1989.

[28] M. Suzuki, H. Yokoyama, S. D. Brorson, E. P. Ippen, *Observation of spontaneous emission lifetime change of dye-containing Langmuir-Blodgett films in optical microcavities*, Appl. Phys. Lett., 58 (10), pp. 998, 1991.

[29] T. J. Rogers, D. G. Deppe, B. G. Streetman, *Effect of an AlAs/GaAs mirror on the spontaneous emission of an InGaAs-GaAs quantum well*, Appl. Phys. Lett., 57 (18), pp. 1858, 1990.

[30] A. F. J. Levi, R. E. Slusher, S. L. McCall, S. J. Pearton, R. A. Logan, *Directional light coupling from microdisk lasers*, Appl. Phys. Lett., 62 (6), pp. 561, 1993.

[31] R. E. Slusher, A. F. J. Levi, U. Mohideen, S. L. McCall, S. J. Pearton, R. A. Logan, *Threshold characteristics of semiconductor microdisk lasers*, Appl. Phys. Lett., 63 (10), pp. 1310, 1993.

[32] E. Yablonovitch, *Photonic band-gap structures*, J. Opt. Sci. Am. B, 10 (2), pp. 283, 1993.

[33] E. Yablonovitch, T. J. Gmitter, *Photonic band structure: the face-centered-cubic case*, Phys. Rev. Lett., 63 (18), pp. 1950, 1989.

[34] E. Yablonovitch, T. J. Gmitter, K. M. Leung, *Photonic band structure: the face-centered-cubic case employing nonspherical atoms*, Phys. Rev. Lett., 67 (17), pp. 2295, 1991.

[35] K. M. Leung, Y. F. Liu, *Full vector wave calculation of photonic band structures in face-centered-cubic dielectric media*, Phys. Rev. Lett., 65 (21), pp. 2646, 1990.

[36] Z. Zhang, S. Satpathy, *Electromagnetic wave propagation in periodic structures: bloch wave solution of Maxwell's equations*, Phys. Rev. Lett., 65 (21), pp. 2650, 1990.

[37] K. M. Ho, T. Chan, C. M. Soukoulis, *Existence of a photonic gap in periodic dielectric structures*, Phys. Rev. Lett., 65 (25), pp. 3152, 1990.

[38] R. D. Meade, K. D. Brommer, A. M. Rappe, J. D. Joannopoulos, *Existence of a photonic band gap in two dimensions*, Appl. Phys. Lett., 61 (4), pp. 495, 1992.

[39] D. R. Smith, R. Dalichaouch, N. Kroll, S. Schultz, S. L. McCall, P. M. Platzman, *Photonic band structure and defects in one and two dimensions*, J. Opt. Soc. Am. B, 10 (2), pp. 314, 1993.

[40] P. L. Gourley, J. R. Wendt, G. A. Vawter, T. M. Brennan, B. E. Hammons, *Optical properties of 2-dimensional photonic lattices fabricated as honeycomb nanostructures in compound semiconductors*, Appl. Phys. Lett., 64 (6), pp. 687, 1994.

[41] W. M. Robertson, G. Arjavalingam, R. D. Meade, K. D. Brommer, A. M. Rappe, J. D. Joannopoulos, *Measurement of photonic band structure in a two-dimensional periodic dielectric array*, Phys. Rev. Lett., 68 (13), pp. 2023, 1992.

[42] B. L. Weiss, G. T. Reed, S. K. Toh, R. A. Soref, and F. Namavar, *Optical waveguides in SIMOX structures*, IEEE Phot. Tech. Lett., 3 (11), pp. 19, 1991.

[43] H. H. Hosack, *Recent progress in SOI materials for the next generation of IC technology*, The Electrochemical Society Interface, pp. 51, Spring 1993.

[44] M. Bruel, Nucl. Inst. Meth. Phys. Res. B, 108, pp. 313, 1996.

[45] P. B. Mumola, et al, *Plasma thinned SOI bonded wafers*, IEEE Intl. SOI Conf. Proc., pp. 152, 1992.

[46] J. S. Foresi, M. R. Black, A. M. Agarwal, and L. C. Kimerling, *Losses in polycrystalline silicon waveguides*, Appl. Phys. Lett., 68 (15), pp. 2052, 1996.

[47] A. M. Agarwal, L. Liao, J. S. Foresi, M. R. Black, X. Duan, and L. C. Kimerling, *Low-loss polycrystalline silicon waveguides for silicon photonics*, J. Appl. Phys., 80 (11), pp. 6120, 1996.

[48] W. B. Jackson, N. M. Johnson, and D. K. Biegelson, *Density of gap states of silicon grain boundaries determined by optical absorption*, Appl. Phys. Lett., 43 (2), pp. 195, 1983.

[49] B. E. Little, *A variational coupled-mode theory including radiation loss for grating-assisted couplers*, J. of Lightwave Tech., 14 (2), pp.188, February 1996.